NACA RM L54E25

NACA

RESEARCH MEMORANDUM

AERODYNAMIC CHARACTERISTICS OF SEVERAL TIP CONTROLS ON A 60° DELTA WING AT A MACH NUMBER OF 1.61

By Douglas R. Lord and K. R. Czarnecki

Langley Aeronautical Laboratory
Langley Field, Va.

NATIONAL ADVISORY COMMITTEE
FOR AERONAUTICS

WASHINGTON

August 5, 1954
Declassified May 16, 1958

NACA RM L54E25

NATIONAL ADVISORY COMMITTEE FOR AERONAUTICS

RESEARCH MEMORANDUM

AERODYNAMIC CHARACTERISTICS OF SEVERAL TIP CONTROLS ON A 60° DELTA WING AT A MACH NUMBER OF 1.61

By Douglas R. Lord and K. R. Czarnecki

SUMMARY

An investigation has been made at a Mach number of 1.61 and a Reynolds number of 4.2×10^6 to determine the control effectiveness characteristics of seven tip controls on a 60° delta wing. Pressure-distribution measurements were made at angles of attack from 0° to 15° for control deflections from -30° to 30°.

Integrated-pressure-distribution results showed that the variations of lift, bending-moment, and pitching-moment coefficients with control deflection were generally linear to ±20°. Although linear theory gave a very good estimate of the basic-wing characteristics due to angle of attack, it overestimated control effectiveness. Moving the hinge line on the half-delta control had little effect on the control effectiveness; however, placing a fence at the wing-control parting line improved the linearity of the effectiveness variations with control deflection for large control deflections.

Correlations of the experimental and theoretical control-effectiveness parameters with control area and control-area moments were obtained which were independent of the control plan forms. Since the largest control possible would be an all-movable wing, extensions of the theoretical correlations were compared to the theoretical basic wing characteristics and found to be in excellent agreement.

INTRODUCTION

As part of a general program of research on controls, an investigation is under way in the Langley 4- by 4-foot supersonic pressure tunnel to determine the important parameters in the design of controls for use on a delta wing at supersonic speeds. The first results of the tests, reported in references 1 and 2, were devoted entirely to tip-control hinge-moment characteristics. Some pressure distributions and control effectiveness characteristics were presented in reference 3 for a full-span trailing-edge control.

The purpose of this report is to present the control effectiveness and hinge-moment characteristics determined from the pressure distributions for the tip-control configurations of reference 1 and the fence configurations of reference 2. The tests were made on a 60° delta wing at a Mach number of 1.61, for a Reynolds number of 4.2×10^6, based on the wing mean aerodynamic chord. The wing angle-of-attack range was from 0° to 12° or 15° and the control deflection range, relative to the wing, was from -30° to 30°.

SYMBOLS

M	stream Mach number
q	stream dynamic pressure
α	wing angle of attack
δ	control deflection relative to wing (positive when control trailing edge is deflected down)
x	distance from wing apex in chordwise direction
y	distance from wing apex in spanwise direction
c_R	wing root chord
$\bar{c}$	wing mean aerodynamic chord
$\bar{c}_c$	control mean aerodynamic chord
$b/2$	wing semispan
S	semispan-wing plan-form area
S_c	control plan-form area
M_B	moment of S_c about wing root
$M_{B(wing)}$	moment of S about wing root
M_A	moment of S_c about y-axis (line through apex perpendicular to the wing root chord)
$M_{A(wing)}$	moment of S about y-axis

L	semispan-wing lift
B	semispan-wing root bending moment
M'	semispan-wing pitching moment about 50-percent station of wing mean aerodynamic chord
M''	semispan-wing pitching moment about y-axis
H	control hinge moment about hinge line
C_L	lift coefficient, $\frac{L}{qS}$
C_b	root bending-moment coefficient, $\frac{B}{2Sbq}$
C_m	pitching-moment coefficient, $\frac{M'}{qS\bar{c}}$
$C_{m'}$	pitching-moment coefficient, $\frac{M''}{qS\bar{c}}$
C_h	control hinge-moment coefficient, $\frac{H}{qS_c\bar{c}_c}$

Slopes:

$$C_{L_\delta} = \frac{\partial C_L}{\partial \delta} \qquad C_{L_\alpha} = \frac{\partial C_L}{\partial \alpha}$$

$$C_{b_\delta} = \frac{\partial C_b}{\partial \delta} \qquad C_{b_\alpha} = \frac{\partial C_b}{\partial \alpha}$$

$$C_{m'_\delta} = \frac{\partial C_{m'}}{\partial \delta} \qquad C_{m'_\alpha} = \frac{\partial C_{m'}}{\partial \alpha}$$

All slopes were obtained at $\alpha = 0^\circ$ and $\delta = 0^\circ$.

APPARATUS

Wind Tunnel

This investigation was conducted in the Langley 4- by 4-foot supersonic pressure tunnel, which is a rectangular, closed-throat, single-return

type of wind tunnel with provisions for the control of the pressure, temperature, and humidity of the enclosed air. For the tests reported herein, the nozzle walls were set for a Mach number of 1.6. At this Mach number, the test section has a width of 4.5 feet and a height of 4.4 feet. During the tests, the stagnation pressure was held at 15 lb/sq in. absolute and the dewpoint was kept below -20° F so that the effects of water condensation in the supersonic nozzle were negligible.

Model and Model Mounting

The model used in this investigation consisted of a half-delta wing having seven interchangeable control surfaces and various associated control adapters (or replacement sections) required to fit the controls to the basic-wing component. Sketches of the seven test configurations are presented in figure 1 with the shaded areas denoting the movable controls. The location of the orifices may be determined from tables I and II and the sketches in figure 2.

The basic wing had a 60° sweptback leading edge, a root chord of 18.14 inches, and a semispan of 10.48 inches. The wing had a rounded NACA 63-series section extending 30 percent root chord back from the leading edge, a constant-thickness center section with a thickness-chord ratio of 3 percent based on the root chord, and a sharp trailing edge. Near the wing tip, the nose section joined directly to the tapered trailing edge without any flat midsection. (See fig. 1.) The wing section remained the same for the different control configurations.

Two types of fences were installed at the wing-control parting line of configuration E for some of the tests as shown in figure 3. The full-chord fence was designed to close the angular gap between the wing and control due to the unporting of the control for a control deflection range of ±30°. The modified fence was made by cutting down the full-chord fence so that only the angular gap ahead of the hinge line was closed. Both fences were attached to the wing. The basic wing and controls were constructed of steel. (For details of construction, see ref. 1.) The fences were made from 1/16-inch stock brass.

The semispan wing was mounted horizontally in the tunnel from a turntable in a steel boundary-layer bypass plate which was located vertically in the test section about 10 inches from the side wall, as shown in figures 4 and 5.

TESTS

The model angle of attack was changed by rotating the turntable in the bypass plate on which the wing was mounted. (See fig. 4.) The angle

of attack was measured by a vernier on the outside of the tunnel, inasmuch as the angular deflection of the wing under load was negligible. Control deflection was changed by a gear mechanism mounted on the pressure box which rotated the strain-gage balance, the torque tube, and the control as a unit. The control angles were set approximately with the aid of an electrical control-position indicator mounted on the torque tube close to the wing root and measured under load during testing with a cathetometer mounted outside the tunnel.

Control hinge moments were determined by means of an electrical strain-gage balance located in the pressure box (fig. 4) which measured the torque on the tube actuating the control surface. The pressure distributions were determined from photographs of the multiple-tube manometer boards to which the pressure leads from the model orifices were connected. The wing lift, pitching-moment, and bending-moment coefficients were determined from integration of the pressure distributions. As a check on the control hinge-moment coefficients measured directly, values were also determined from the integrated pressure distributions.

Tests were made over an angle-of-attack range from 0° to 12° or 15°, at increments of either 3° or 6°. The control-deflection range was from -30° to 30°, with hinge moments measured every 5° and pressures measured every 10°. All tests were made at a tunnel stagnation pressure of 15 lb/sq in absolute, corresponding to a Reynolds number, based on the mean aerodynamic chord of 12.10 inches, of 4.2×10^6.

PRECISION OF DATA

The mean Mach number in the region occupied by the model is estimated from calibration to be 1.61 with local variations being smaller than ±0.02. There is no evidence of any significant flow angularities. The overall accuracies of the integrated coefficients are not known; however, if the pressure-distribution fairings are assumed to be correct, the repeatability of the integrated coefficients and the estimated accuracies of other pertinent quantities are:

α, deg	±0.05
δ, deg	±0.1
C_L (from integrations)	±0.01
C_b (from integrations)	±0.0025
C_m (from integrations)	±0.0025
C_h (from direct measurements)	±0.005

RESULTS AND DISCUSSION

Effect of Control Deflection

The basic test data are presented in figures 6 to 14 for the seven control configurations and the two fence configurations in the form of variations of wing lift, bending-moment, and pitching-moment and control hinge-moment coefficients with control deflection. The solid curves were obtained from the pressure-distribution measurements and the dotted hinge-moment-coefficient curves were obtained from the strain-gage measurements. The latter were presented previously in reference 1 and are presented herein merely to give an indication of the reliability of the pressure-distribution integrations. In consideration of the small number of pressure orifices on each surface, the integrated hinge-moment coefficients are in remarkably good agreement with those measured directly. The largest discrepancies seem to be on the fence configurations, possibly because the fences may introduce pressure changes that could not be accurately determined from the limited pressure distributions.

The variations of lift and bending-moment coefficient with control deflection (figs. 6 to 14) are generally parallel at the different angles of attack for each of the test configurations. The lift and bending-moment effectivenesses tend to decrease at large values of control deflection for most of the models. The curves of pitching-moment coefficient converge at the negative control deflections due to a decreased pitching-moment effectiveness at positive angles of attack. The loss in pitching-moment effectiveness at large control deflections is generally less pronounced than is the loss in lift and bending-moment effectiveness. The variations with control deflection of the hinge-moment coefficients were discussed in detail in reference 1 and are therefore not repeated here.

Effect of Wing Angle of Attack

The experimental and theoretical variations of the basic-wing ($\delta = 0^\circ$) lift, bending-moment, and pitching-moment coefficients with angle of attack are presented in figure 15. These curves were obtained from the cross plots of the curves of figures 6 to 14 with the exception of configuration D and the fence configurations. The theoretical predictions here and throughout this paper were obtained by linear-theory methods such as those in references 4 to 6.

Linear theory predicts the lift- and bending-moment-coefficient slopes very well at the low angles of attack. The pitching-moment prediction appears to be poor but in reality is very good since the choice of the pitch center at the wing centroid magnifies the discrepancy. The moment increment is equivalent to a center-of-pressure shift of about 3 percent of the wing mean aerodynamic chord.

The experimental variations of the wing characteristics with angle of attack show a gradual decrease in slopes as the angle of attack is increased. The variations at the other test control deflections, although not presented here, exhibit the same general behavior.

Effect of Hinge-Line Location

Control configurations E, F, and G were identical except for the location of the hinge lines. It is of interest therefore to compare the variations of wing lift, bending-moment, and pitching-moment coefficients with control deflection as shown in figure 16. Although there are some small differences in the curves, there are no systematic changes with movement of the hinge line. As reported in reference 1, the control hinge moments varied with the balance ratio, and it appears to be possible to balance the hinge moments, for small deflections, of a half-delta tip control by proper placement of the hinge line without adversely affecting the control effectiveness.

Effect of Fences

The variation of the wing lift, bending-moment, and pitching-moment coefficients with control deflection for configuration E with and without the fences mounted at the wing-control parting line is shown in figure 17. Although there seems to be little effect of the fences on the control effectiveness over most of the range, the fences tend to increase the linearity of the variations with control deflection at the large control deflections. In view of the linearizing effect of the fences on the hinge-moment variations (see ref. 2), the outlook for fences of the type investigated is encouraging from all but the drag standpoint.

Effect of Control Size and Location

Correlations of the experimental and theoretical wing lift-, bending-moment-, and pitching-moment-coefficient slopes due to control deflection as functions of control-to-wing ratios of area, area moment about the root chord, and area moment about the wing apex, respectively, are presented in figure 18 for the seven basic configurations. In addition, points are included for a full-span trailing-edge control from reference 3 and a small half-delta tip control from reference 7. Both the theoretical and experimental points correlate on approximately straight lines, the slopes of the experimental correlations being about 77 percent of the corresponding theoretical correlations. The agreement between the theoretical and experimental correlations might be expected to improve if the theoretical calculations were corrected for thickness (ref. 8). The

experimental correlations presented here were presented previously in reference 9. Similar correlations were obtained on a trapezoidal wing at Mach numbers of 1.61 and 2.01 in reference 8.

It can be shown theoretically that, if the control size is increased, the control characteristics will eventually approach the wing characteristics. In figure 19, the theoretical correlations of figure 18 are compared with straight lines drawn from the origin through the points representing the theoretical wing lift-, bending-moment-, and pitching-moment-coefficient slopes with angle of attack. The agreement between the theoretical correlation of figure 18 and the line just described is very good and indicates that to a first approximation the theoretical characteristics for similar controls on the wing can be obtained quickly from the theoretical basic-wing characteristics. Within the range of experimental area and area-moment ratios tested, figure 18 can then be used to correct the results to values that can be expected experimentally at moderate control deflections.

A similar comparison of the correlated control characteristics with the basic-wing characteristics was made purely on an experimental basis. The agreement between the wing and the correlated control characteristics in this case, however, was not so good as the theoretical comparison. The reason lies in the fact that within the range of control sizes studied in this investigation, linear theory considerably overestimates the control effectiveness but is in good agreement with the experimental results for the complete wing. On a physical basis a possible explanation is that the chordwise extent of the flow separation at the trailing edge is approximately constant, whether induced by control deflection or angle of attack, and that percentagewise the effects are much less when based on the wing area or moment than when based on the much smaller control area or moment.

CONCLUSIONS

An investigation has been made at a Mach number of 1.61 and a Reynolds number of 4.2×10^6 to determine the control effectiveness characteristics of seven tip controls on a 60° delta wing. Tests were made at angles of attack from 0° to 15° for control deflections from -30° to 30° and the results indicate the following conclusions:

1. The lift-, bending-moment-, and pitching-moment-coefficient variations with control deflection were generally linear to $\pm 20^\circ$. The linear theory overestimated the control effectiveness but gave a very good estimete of the basic-wing characteristics due to angle of attack.

2. On a half-delta tip control, the hinge line can be placed to balance the hinge moments due to control deflection without appreciably affecting the control effectiveness.

3. Placing a fence at the wing-control parting line of one of the half-delta controls had a small linearizing effect on the control effectiveness variations in the range of large control deflections.

4. Correlations of the experimental and theoretical control-effectiveness parameters with control area and control-area moments were obtained which were independent of the control plan forms. Since the largest control possible would be an all-movable wing, extensions of the theoretical correlations were compared to the theoretical basic wing characteristics and found to be in excellent agreement.

Langley Aeronautical Laboratory,
National Advisory Committee for Aeronautics,
Langley Field, Va., May 13, 1954.

REFERENCES

1. Czarnecki, K. R., and Lord, Douglas R.: Hinge-Moment Characteristics for Several Tip Controls on a 60° Sweptback Delta Wing at Mach Number 1.61. NACA RM L52K28, 1953.

2. Czarnecki, K. R., and Lord, Douglas R.: Preliminary Investigation of the Effect of Fences and Balancing Tabs on the Hinge-Moment Characteristics of a Tip Control on a 60° Delta Wing at Mach Number 1.61. NACA RM L53D14, 1953.

3. Lord, Douglas R., and Czarnecki, K. R.: Aerodynamic Characteristics of a Full-Span Trailing-Edge Control on a 60° Delta Wing With and Without a Spoiler at a Mach Number of 1.61. NACA RM L53L17, 1954.

4. Lagerstrom, P. A., and Graham, Martha E.: Linearized Theory of Supersonic Control Surfaces. Jour. Aero. Sci., vol. 16, no. 1, Jan. 1949, pp. 31-34.

5. Tucker, Warren A., and Nelson, Robert L.: Theoretical Characteristics in Supersonic Flow of Two Types of Control Surfaces on Triangular Wings. NACA Rep. 939, 1949. (Supersedes NACA TN's 1600, 1601, and 1660.)

6. Kainer, Julian H., and King, Mary Dowd: The Theoretical Characteristics of Triangular-Tip Control Surfaces at Supersonic Speeds. Mach Lines Behind Trailing Edges. NACA TN 2715, 1952.

7. Guy, Lawrence D.: Control Hinge-Moment and Effectiveness Characteristics of a 60° Half-Delta Tip Control on a 60° Delta Wing at Mach Numbers of 1.41 and 1.96. NACA RM L52H13, 1952.

8. Lord, Douglas R., and Czarnecki, K. R.: Aerodynamic Characteristics of Several Flap-Type Trailing-Edge Controls on a Trapezoidal Wing at Mach Numbers of 1.61 and 2.01. NACA RM L54D19, 1954.

9. Lord, Douglas R., and Czarnecki, K. R.: Recent Information on Flap and Tip Controls. NACA RM L53I17a, 1953.

TABLE I

SPANWISE LOCATION OF ORIFICE STATIONS

[Chordwise extent of stations shown in fig. 2 and table II]

Configuration	Values of 2y/b								
	Sta. 1	Sta. 2	Sta. 3	Sta. 4	Sta. 5	Sta. 6	Sta. 7	Sta. 8	Sta. 9
A	0.048	0.210	0.372	0.537	0.592	0.745	0.860	See fig. 2	-----
B	.048	.210	.372	.537	See fig. 2	.602	See fig. 2	0.734	See fig. 2
C	.048	.210	.372	.537	.601	.640	.683	.758	See fig. 2
D	.055	.242	.430	.619	.688	.776	.876	.958	-----
E	.048	.210	.372	.537	.597	.733	.869	.967	-----
F	.048	.210	.372	.537	.597	.733	.869	.967	-----
G	.048	.210	.372	.537	.597	.733	.869	.967	-----

TABLE II

CHORDWISE LOCATION OF ORIFICES

(a) Configuration A.

[Orifice locations identical on upper and lower surfaces; station spanwise locations shown in fig. 2 and in table I]

Orifice	Values of x/c_R							
	Sta. 1	Sta. 2	Sta. 3	Sta. 4	Sta. 5 (a)	Sta. 6 (a)	Sta. 7	Sta. 8 (a)
1	0.048	0.210	0.372	0.535	0.592	0.745	0.872	0.872
2	.075	.238	.400	.562	.619	.772	.919	.919
3	.219	.381	.538	.700	.713	.816	.952	.952
4	.334	.502	.659	.860	.779	.860	.982	.982
5	.445	.612	.747	.897	.860	.872		
6	.588	.756	.860	.936	.872	.919		
7	.742	.860	.897	.985	.919	.952		
8	.860	.897	.936		.952	.982		
9	.897	.936	.985		.982			
10	.936	.985						
11	.985							

[a]Additional orifices located on control leading edge at stations 5, 6, and 8.

TABLE II - Continued

CHORDWISE LOCATION OF ORIFICES

(b) Configuration B.

[Orifice locations identical on upper and lower surfaces; station spanwise locations shown in fig. 2 and in table I]

Orifice (a)	Values of x/c_R								
	Sta. 1	Sta. 2	Sta. 3	Sta. 4	Sta. 5	Sta. 6	Sta. 7	Sta. 8	Sta. 9
1	0.048	0.210	0.372	0.535	0.708	0.875	0.754	0.769	0.819
2	.075	.238	.400	.562	.761	.906	.799	.824	.871
3	.219	.381	.538	.700	.810	.945	.835	.879	.926
4	.334	.502	.659	.846		.986		.934	.988
5	.445	.612	.747	.901				.992	
6	.588	.756	.846	.950					
7	.742	.846	.901	.986					
8	.846	.901	.950						
9	.901	.950	.986						
10	.950	.986							
11	.986								

[a]Additional orifice located on control inner leading edge at $\frac{x}{c_R} = 0.767$.

TABLE II - Continued

CHORDWISE LOCATION OF ORIFICES

(c) Configuration C.

[Orifice locations identical on upper and lower surfaces; station spanwise locations shown in fig. 2 and in table I]

Orifice	Values of x/c_R								
	Sta. 1	Sta. 2	Sta. 3	Sta. 4	Sta. 5	Sta. 6	Sta. 7	Sta. 8	Sta. 9
1	0.048	0.210	0.372	0.535	0.876	0.674	0.683	0.758	0.871
2	.075	.238	.400	.562	.909	.769	.711	.785	.928
3	.219	.381	.538	.700	.947	.857	.780	.879	.986
4	.334	.502	.659	.846	.991		.876	.929	
5	.445	.612	.747	.901				.992	
6	.588	.756	.846	.950					
7	.742	.846	.901	.986					
8	.846	.901	.950						
9	.901	.950	.986						
10	.950	.986							
11	.986								

TABLE II - Continued

CHORDWISE LOCATION OF ORIFICES

(d) Configuration D.

[Orifice locations identical on upper and lower surfaces; station spanwise locations shown in fig. 2 and in table I]

Orifice	Values of x/c_R							
	Sta. 1	Sta. 2	Sta. 3	Sta. 4	Sta. 5	Sta. 6	Sta. 7	Sta. 8
1	0.048	0.210	0.372	0.535	0.595	0.672	0.758	0.862
2	.075	.238	.400	.562	.623	.699	.785	
3	.219	.381	.538	.700	.675	.752	.813	
4	.334	.502	.659	.846	.744	.826	.851	
5	.445	.612	.747	.901	.821	.876	.901	
6	.588	.756	.846	.950	.899	.937		
7	.742	.846	.901	.984	.970			
8	.846	.901	.950					
9	.901	.950	.984					
10	.950	.984						
11	.984							

TABLE II - Concluded

CHORDWISE LOCATION OF ORIFICES

(e) Configurations E, F, and G.

[Orifice locations identical on upper and lower surfaces; station spanwise locations shown in fig. 2 and in table I]

Orifice	Values of x/c_R							
	Sta. 1	Sta. 2	Sta. 3	Sta. 4	Sta. 5	Sta. 6	Sta. 7	Sta. 8
1	0.048	0.210	0.372	0.535	0.597	0.730	0.864	0.987
2	.075	.238	.400	.562	.625	.758	.892	
3	.219	.381	.538	.700	.674	.808	.941	
4	.334	.502	.659	.846	.746	.879	.986	
5	.445	.612	.747	.901	.840	.973		
6	.588	.756	.846	.950	.939			
7	.742	.846	.901	.984	.988			
8	.846	.901	.950					
9	.901	.950	.984					
10	.950	.984						
11	.984							

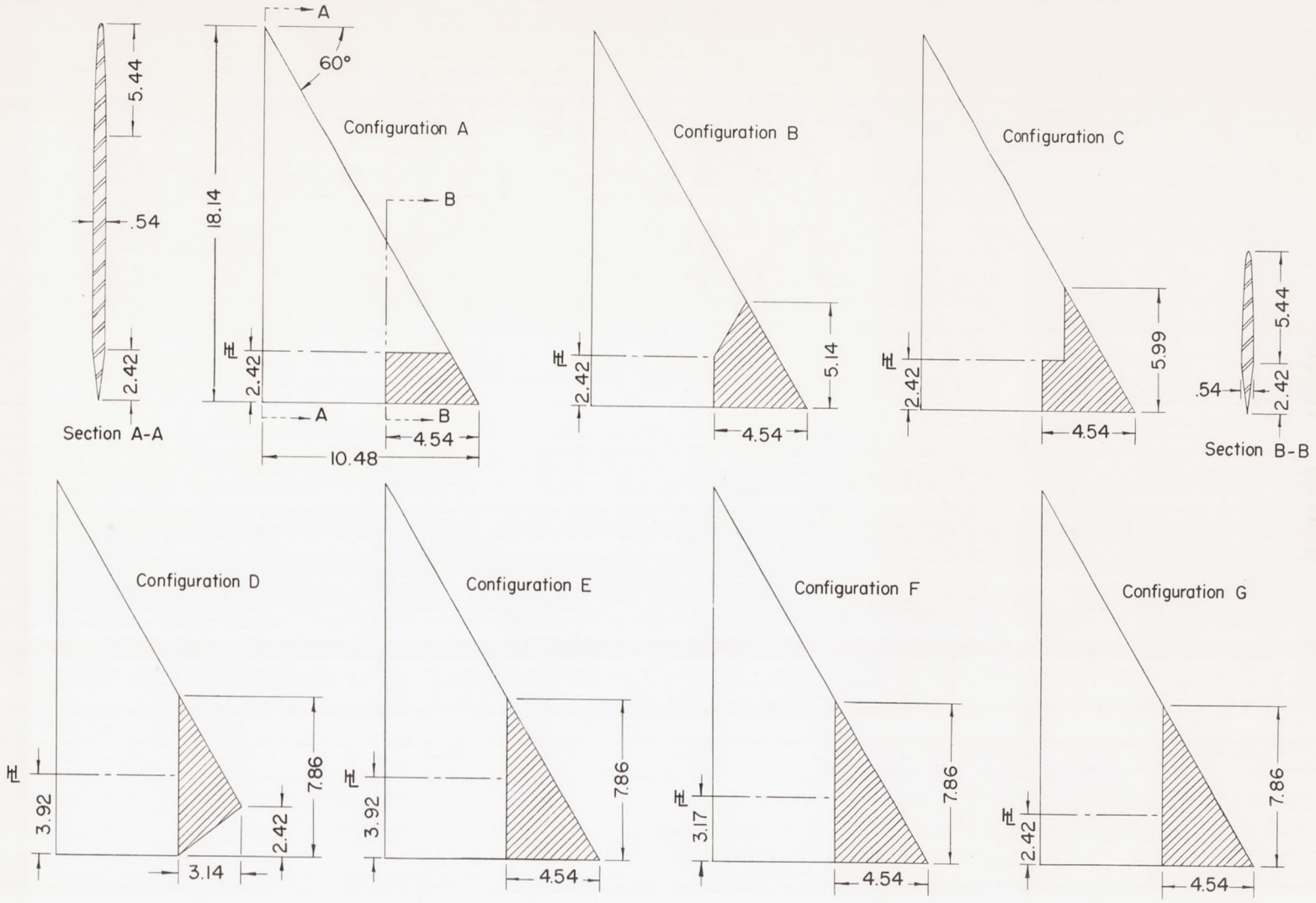

Figure 1.- Sketches of the basic model configurations. (All dimensions in inches.)

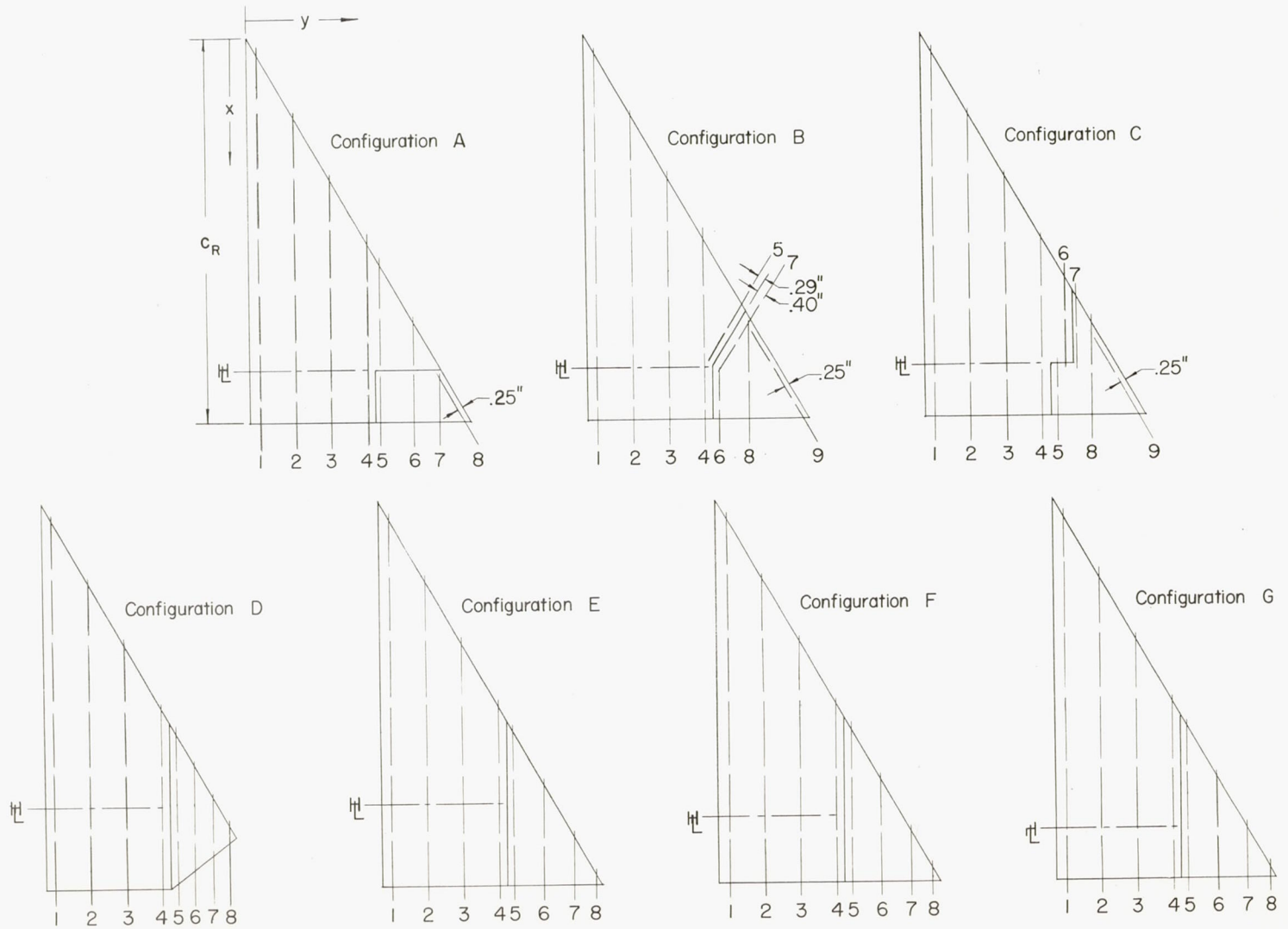

Figure 2.- Sketches of the orifice-station locations.

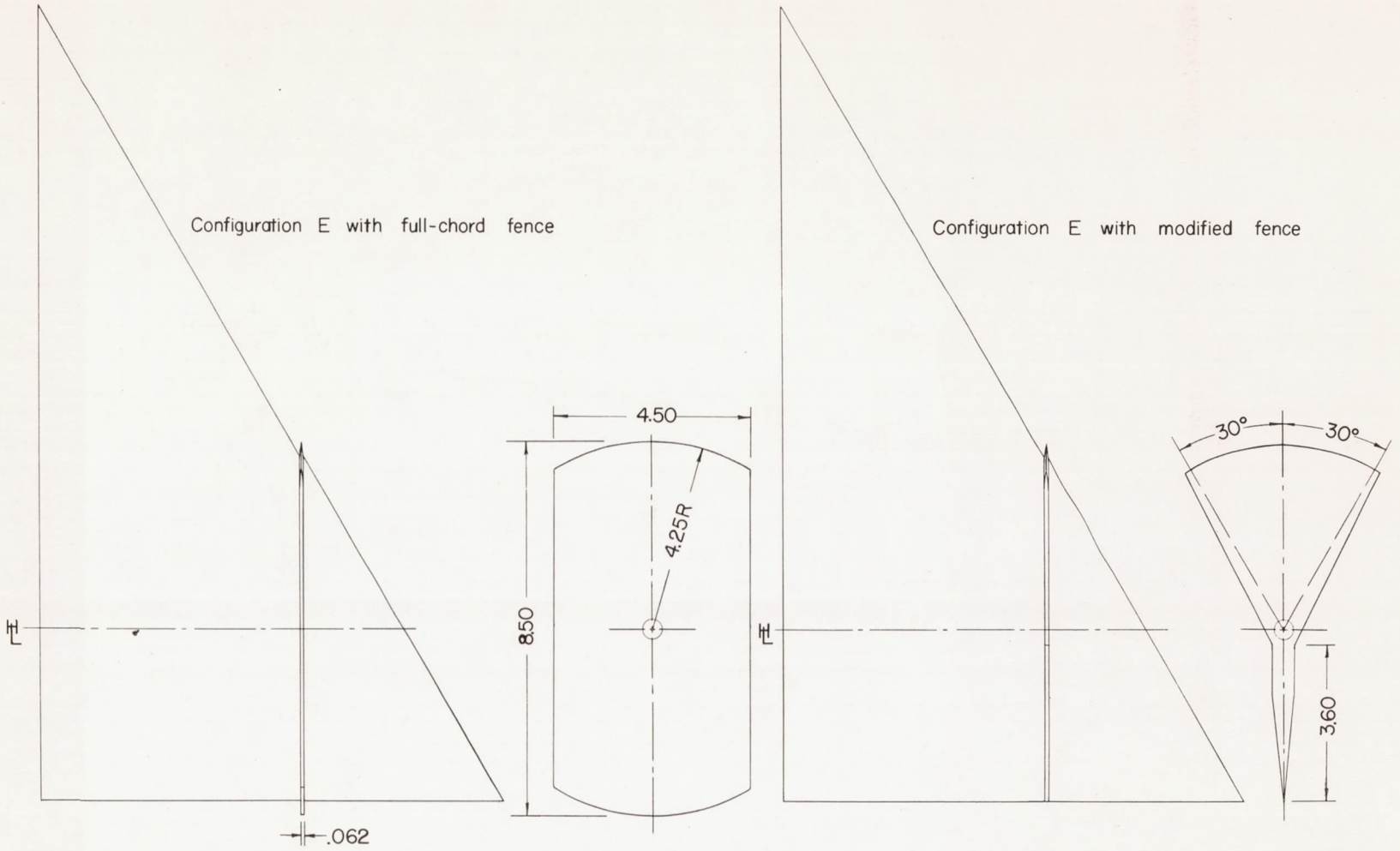

Figure 3.- Sketches of the fence configurations.

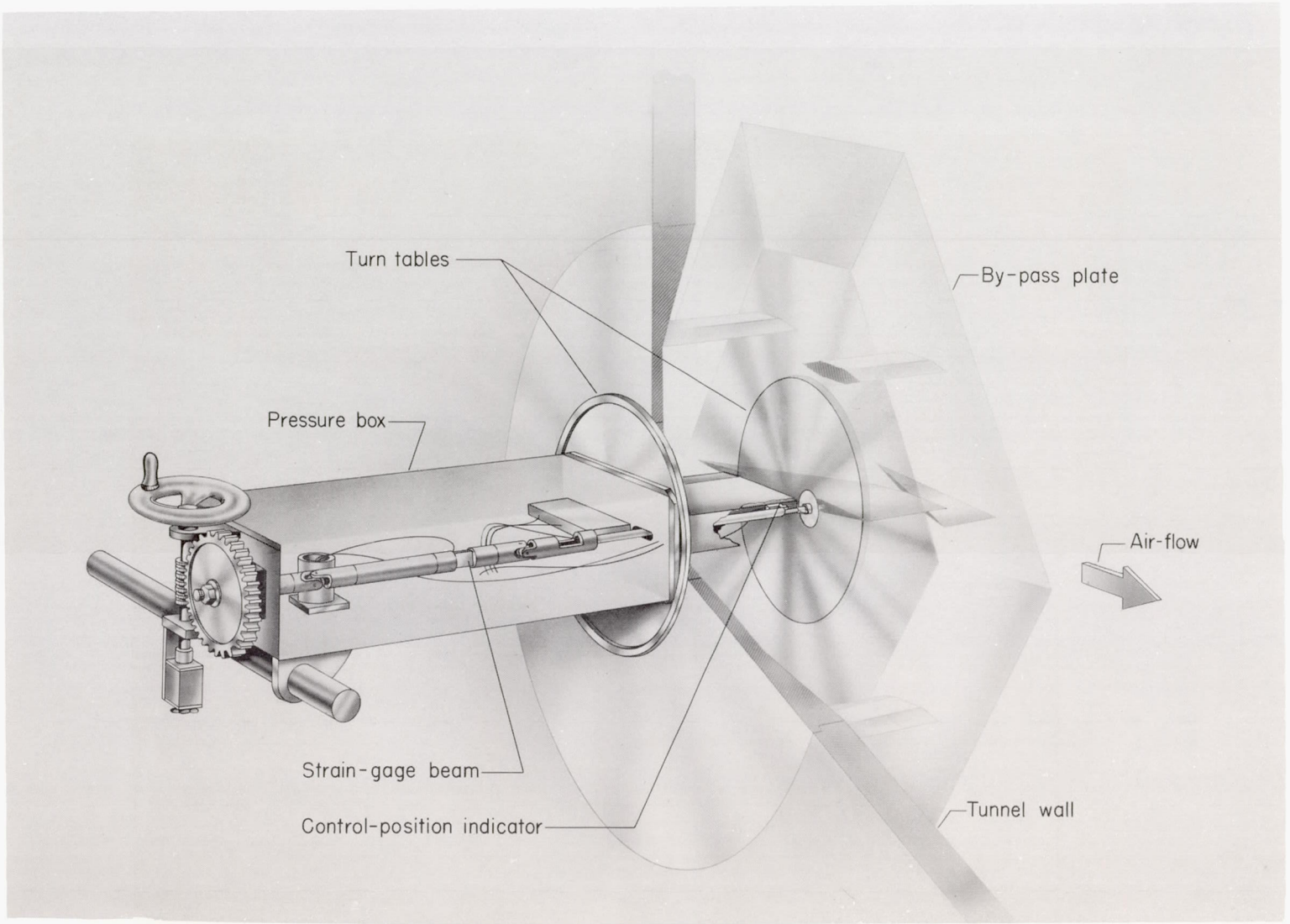

Figure 4.- Sketch of the test setup.

L-77038

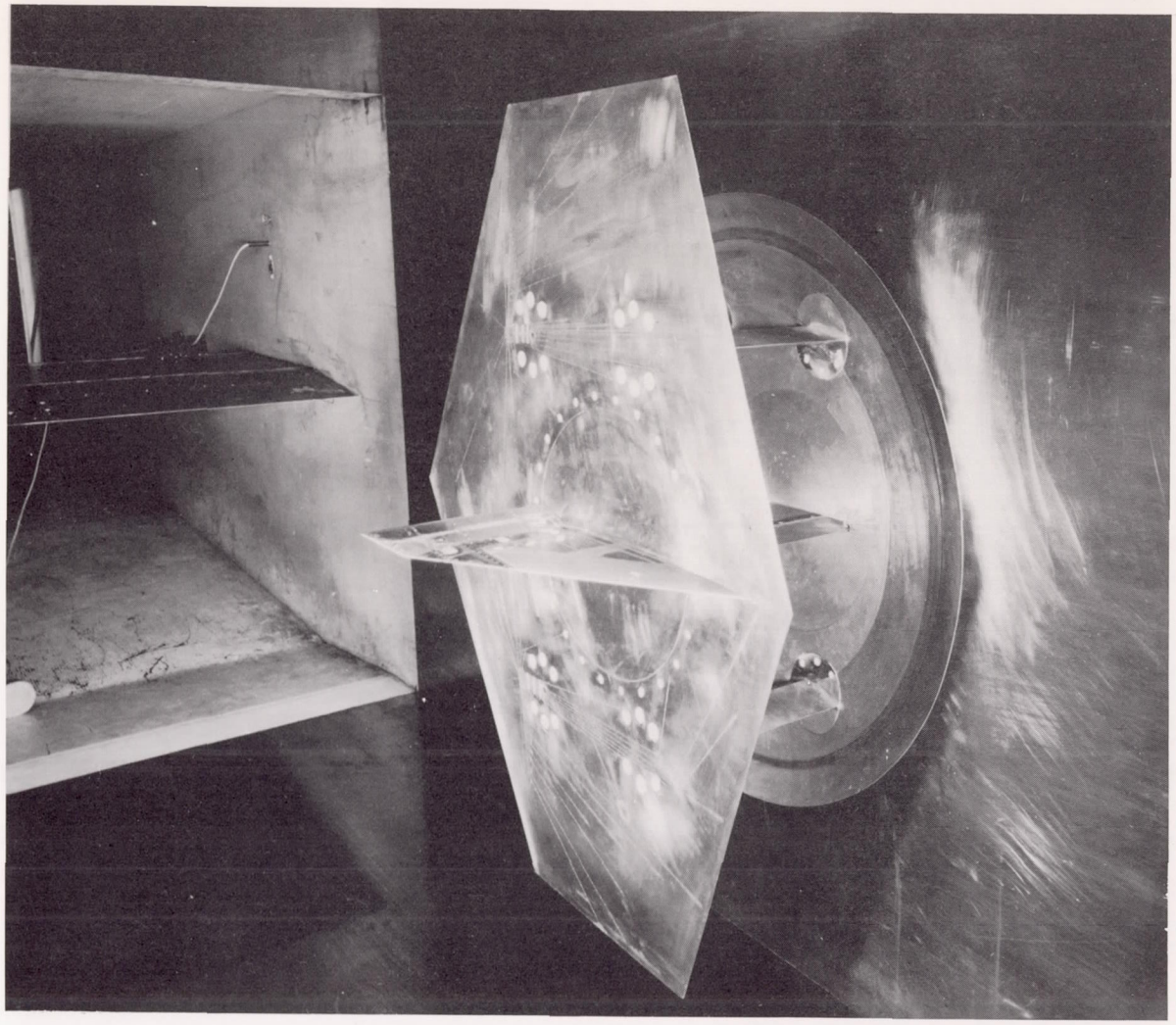

L-75294

Figure 5.- Semispan delta-wing model mounted in tunnel on boundary-layer bypass plate. (Full-span trailing-edge-control configuration shown.)

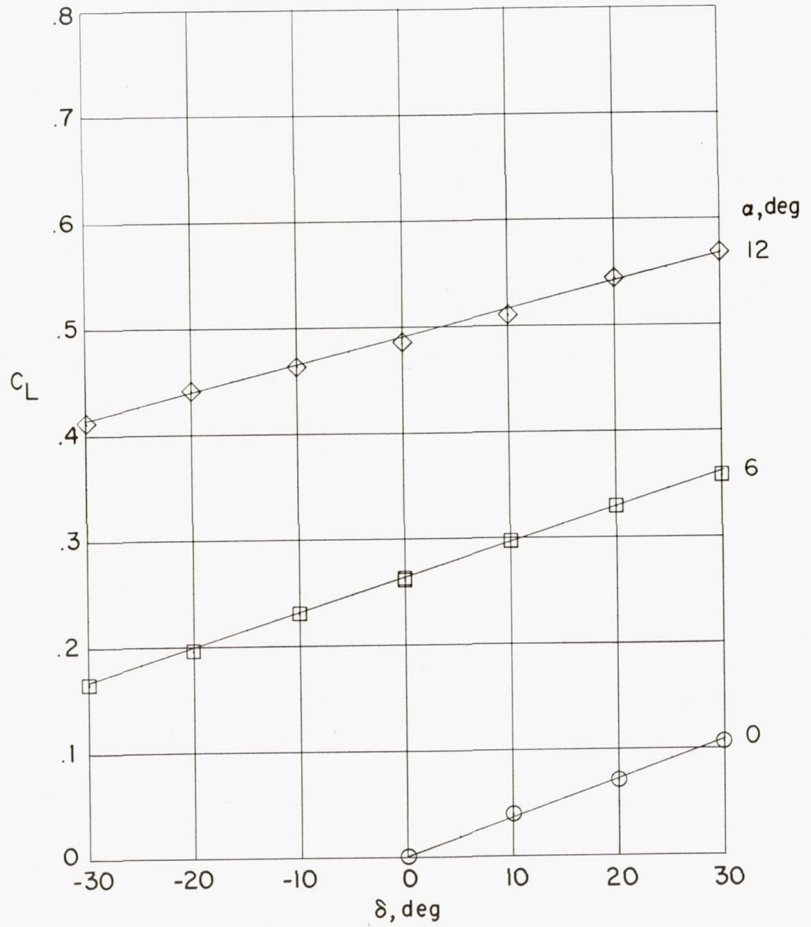

(a) C_L.

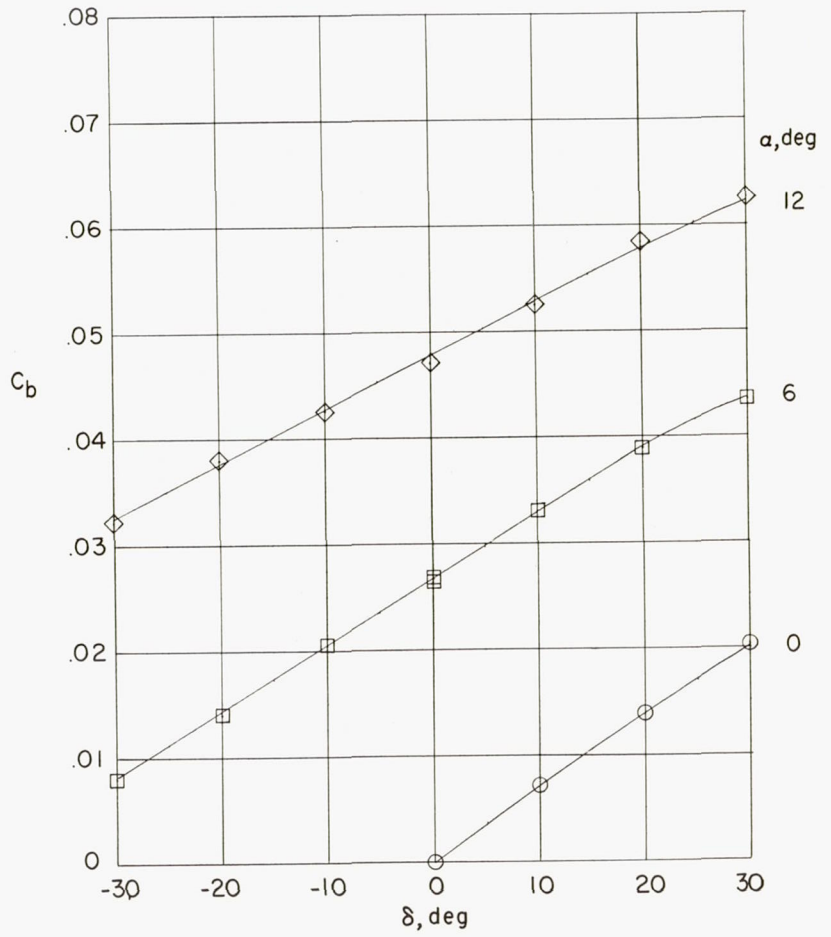

(b) C_b.

Figure 6.- Variation of basic coefficients with control deflection for configuration A.

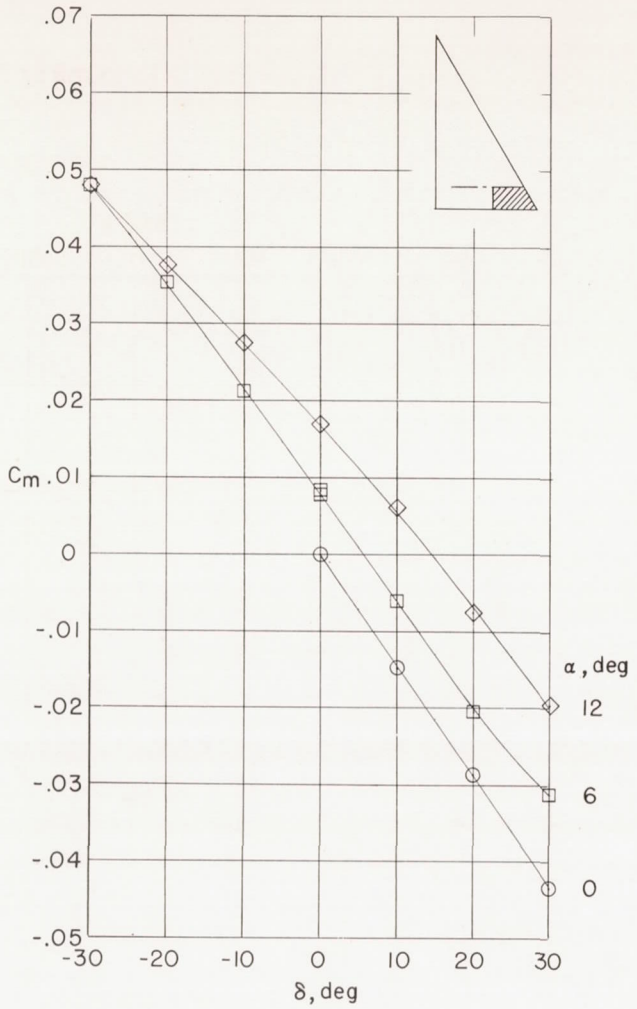

(c) C_m.

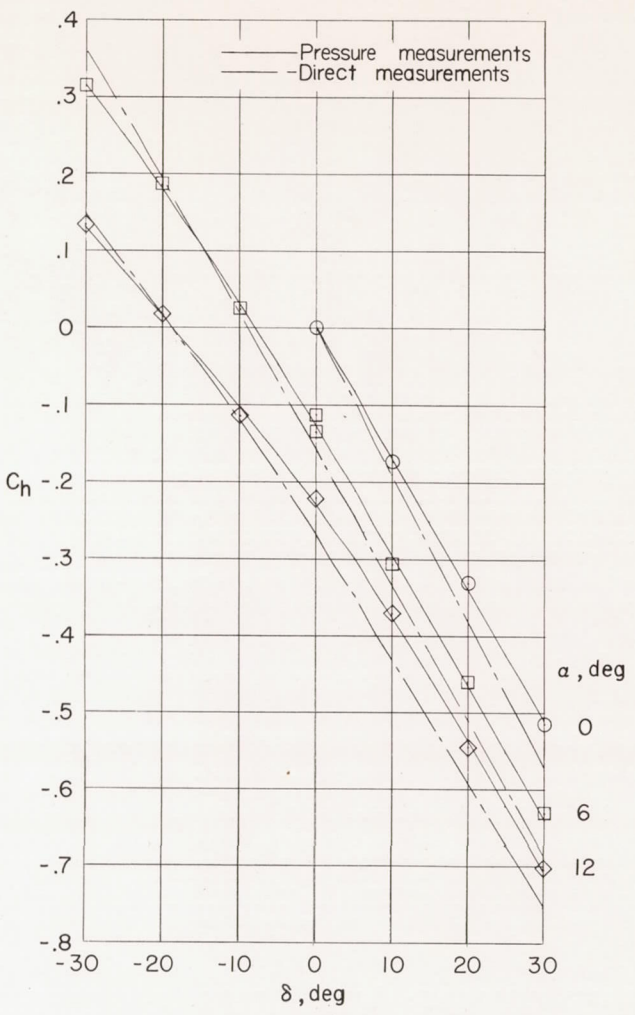

(d) C_h.

Figure 6.- Concluded.

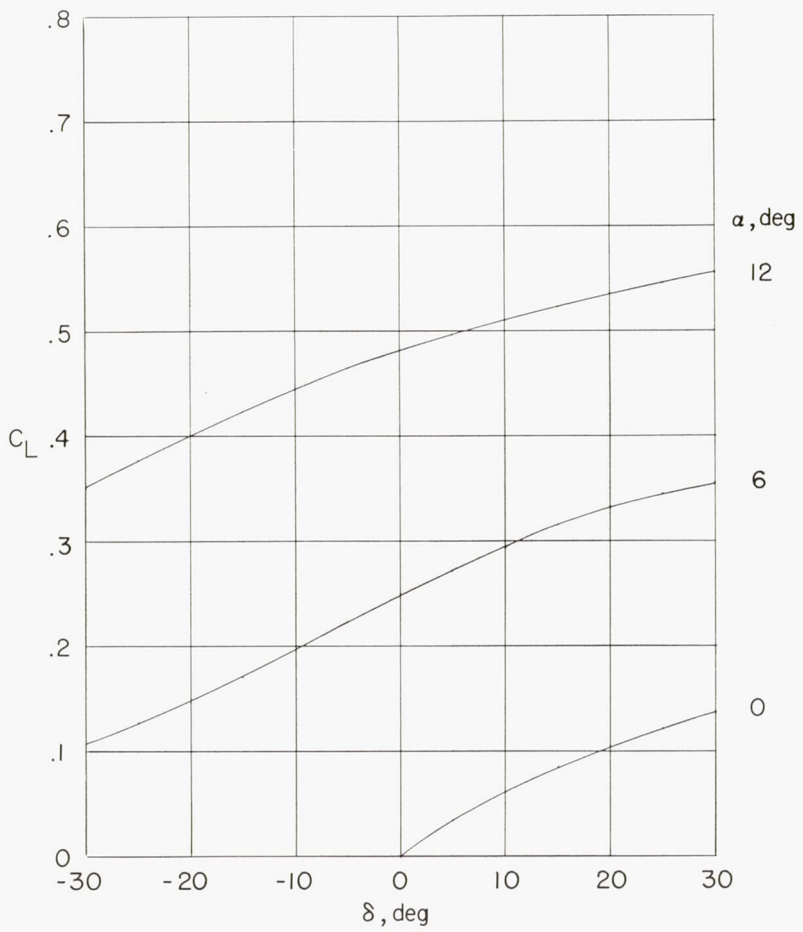

(a) C_L.

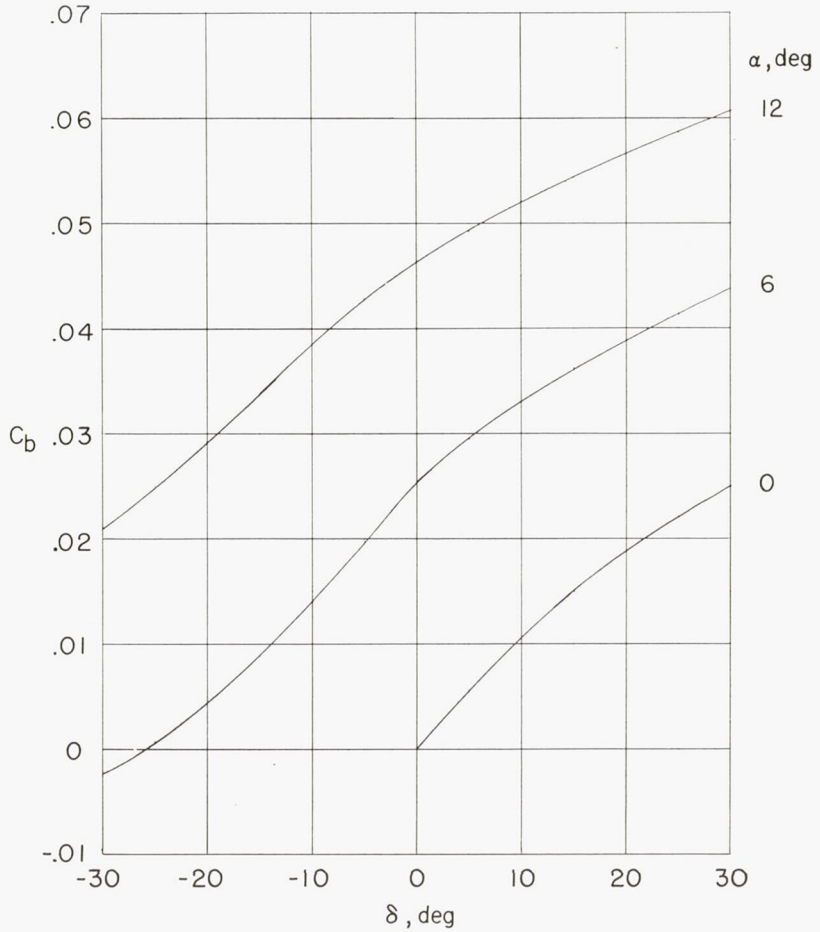

(b) C_b.

Figure 7.- Variation of basic coefficients with control deflection for configuration B.

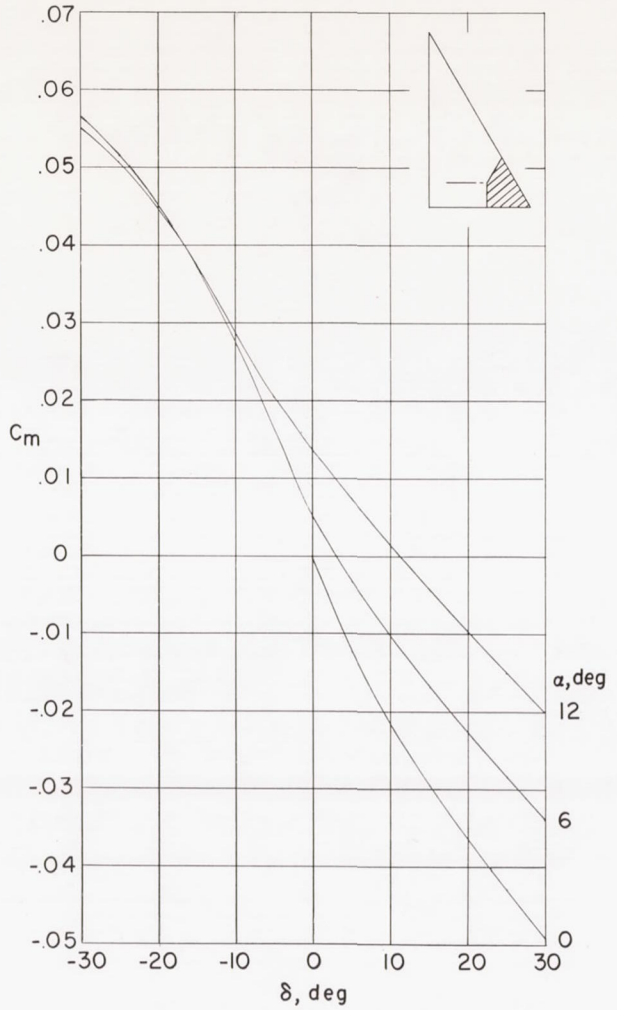

(c) C_m.

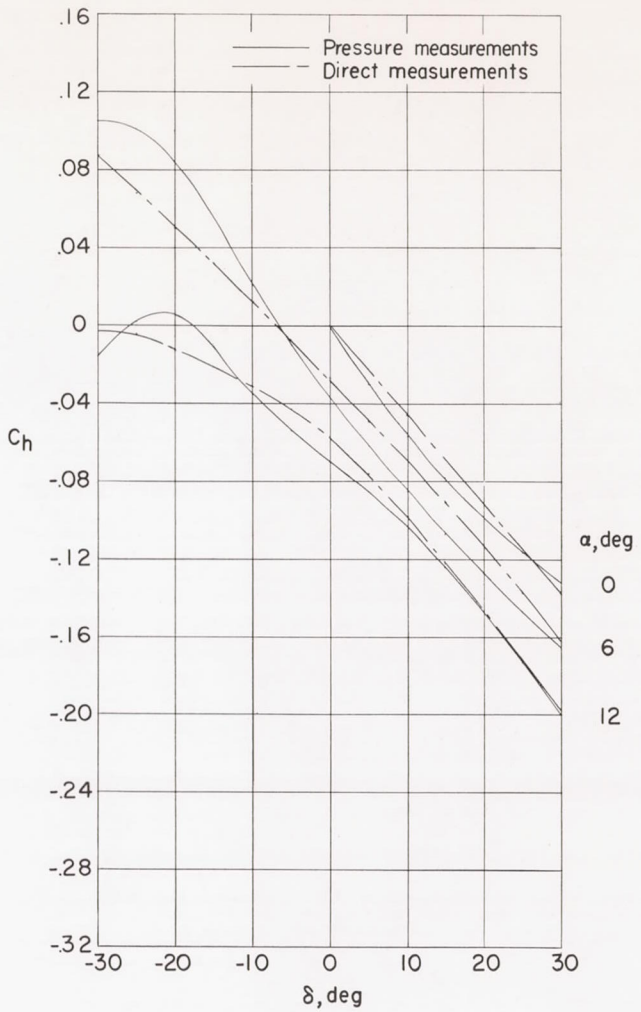

(d) C_h.

Figure 7.- Concluded.

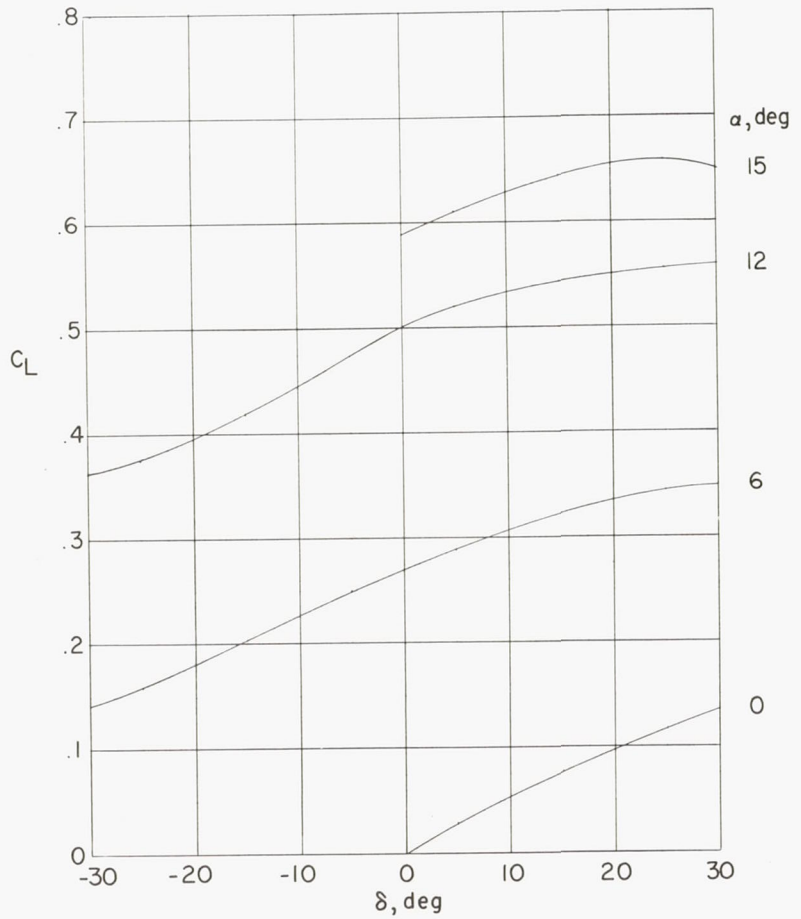

(a) C_L.

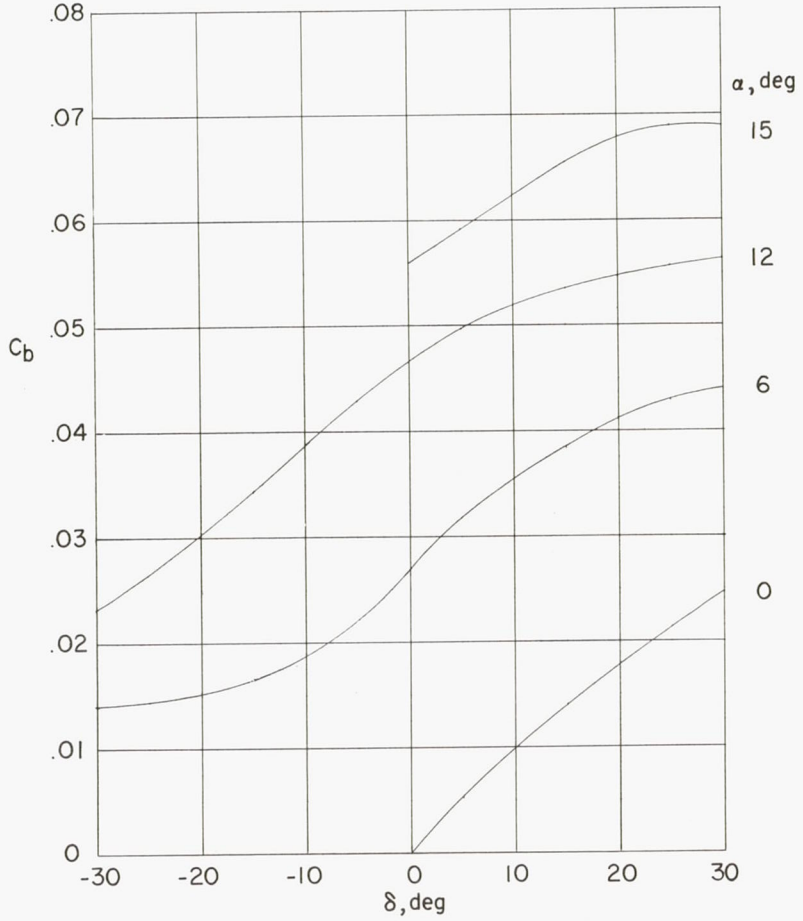

(b) C_b.

Figure 8.- Variation of basic coefficients with control deflection for configuration C.

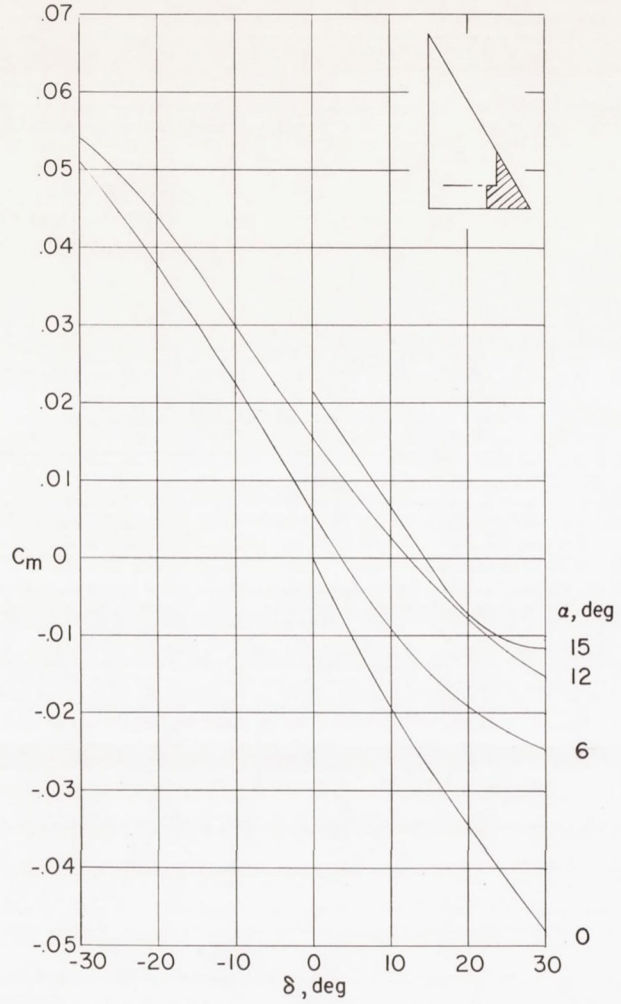

(c) C_m.

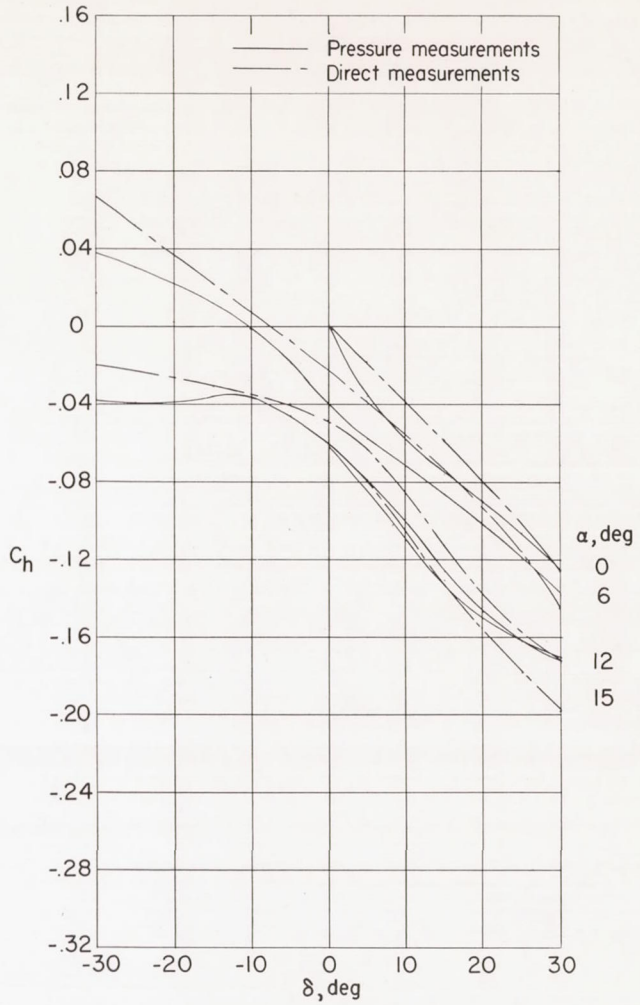

(d) C_h.

Figure 8.- Concluded.

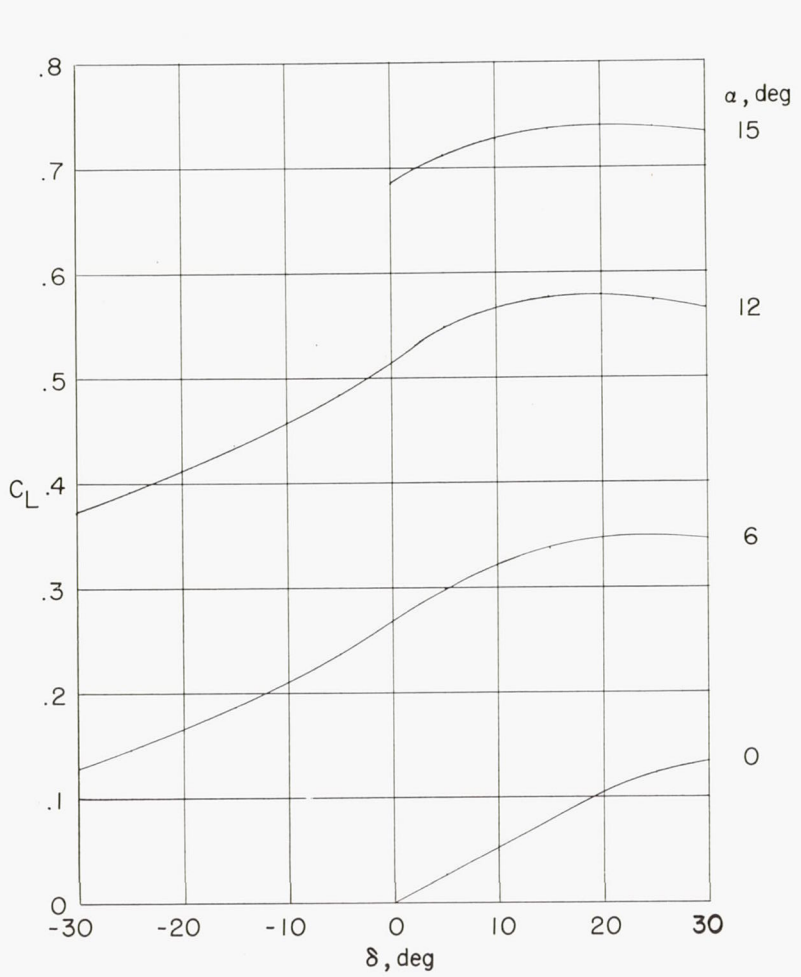

(a) C_L.

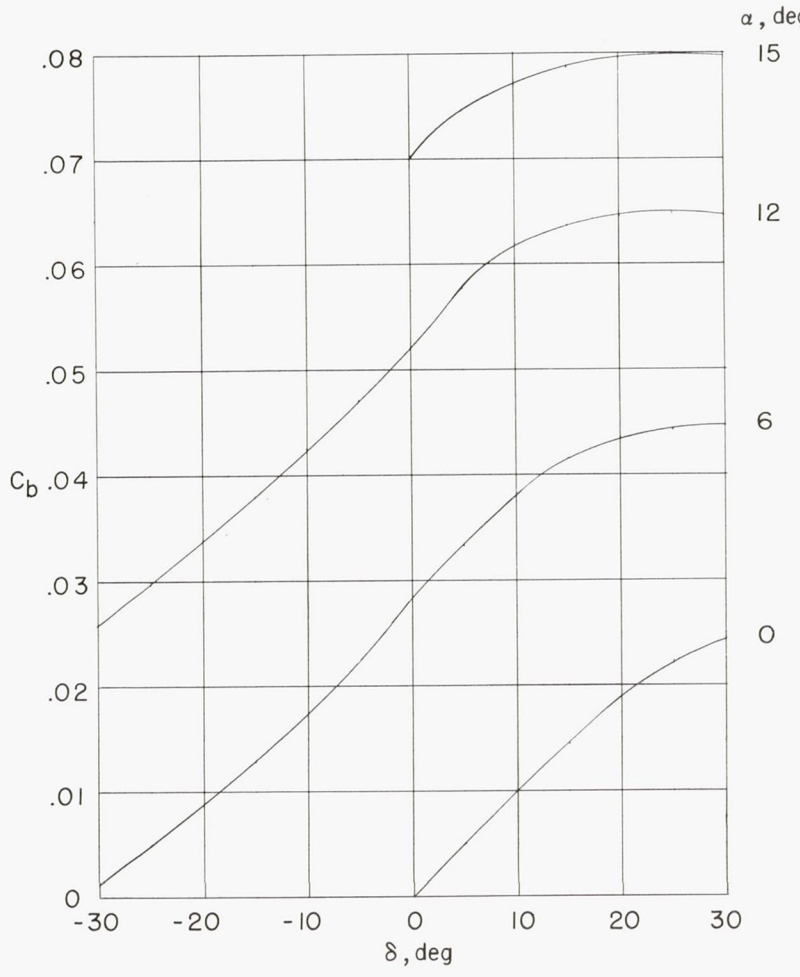

(b) C_b.

Figure 9.- Variation of basic coefficients with control deflection for configuration D.

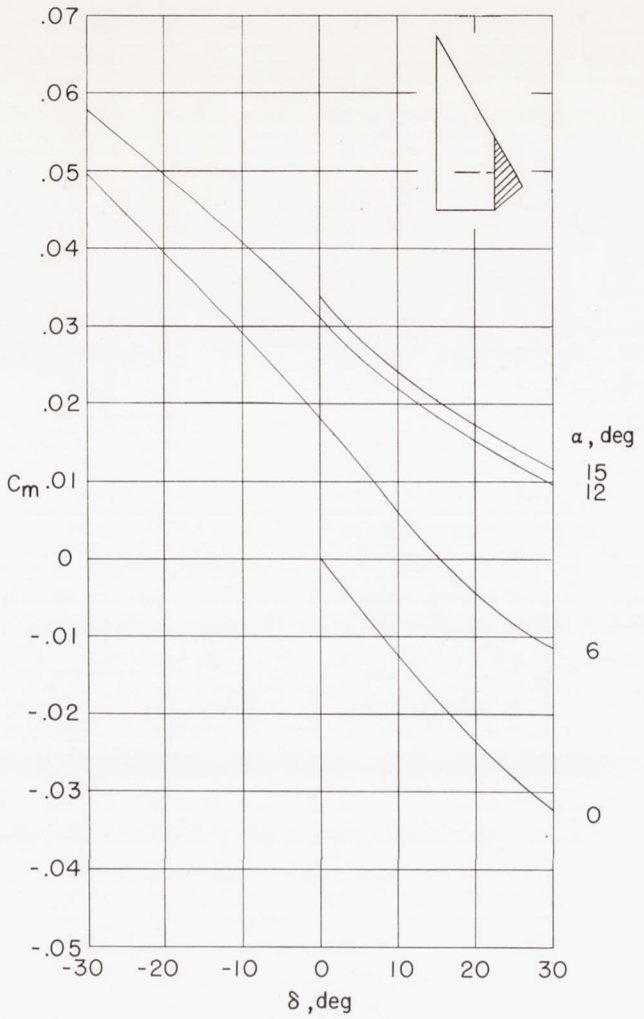

(c) C_m.

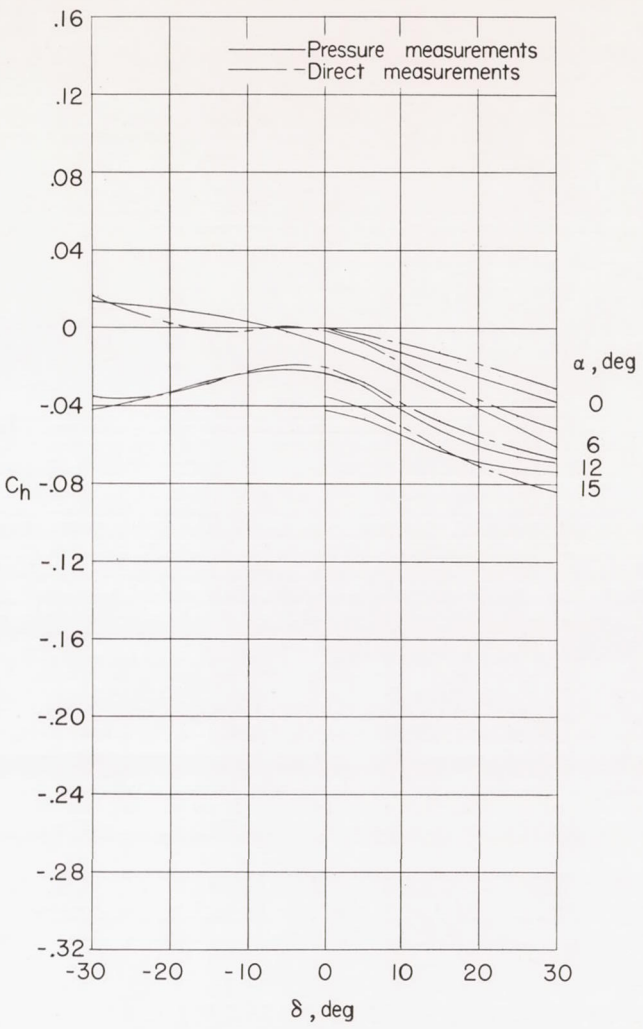

(d) C_h.

Figure 9.- Concluded.

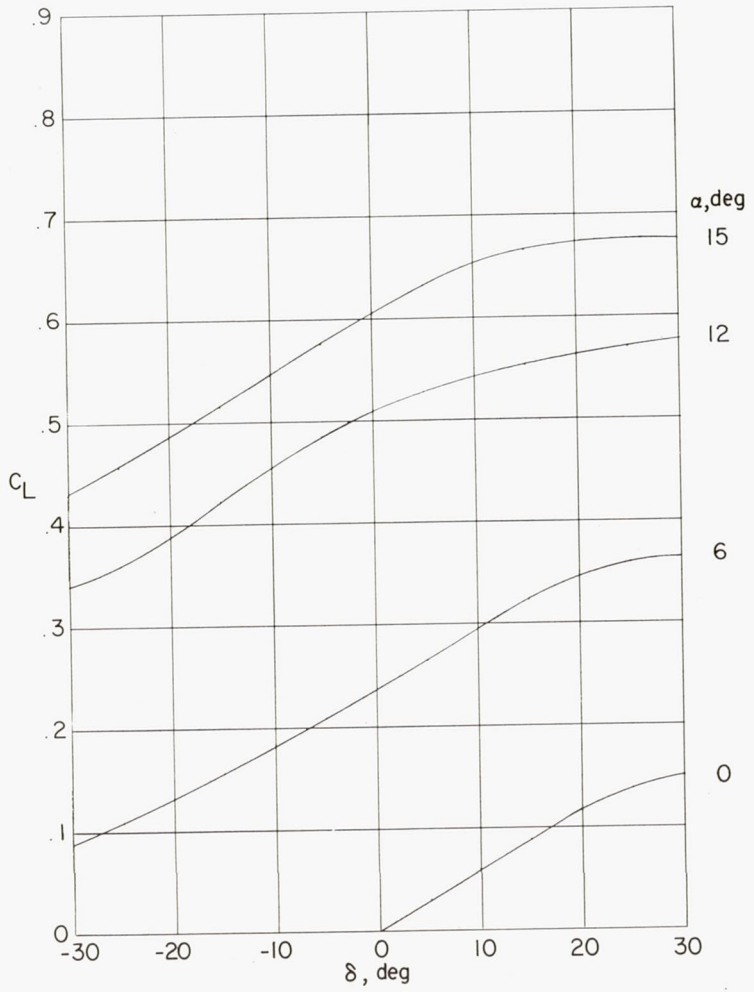

(a) C_L.

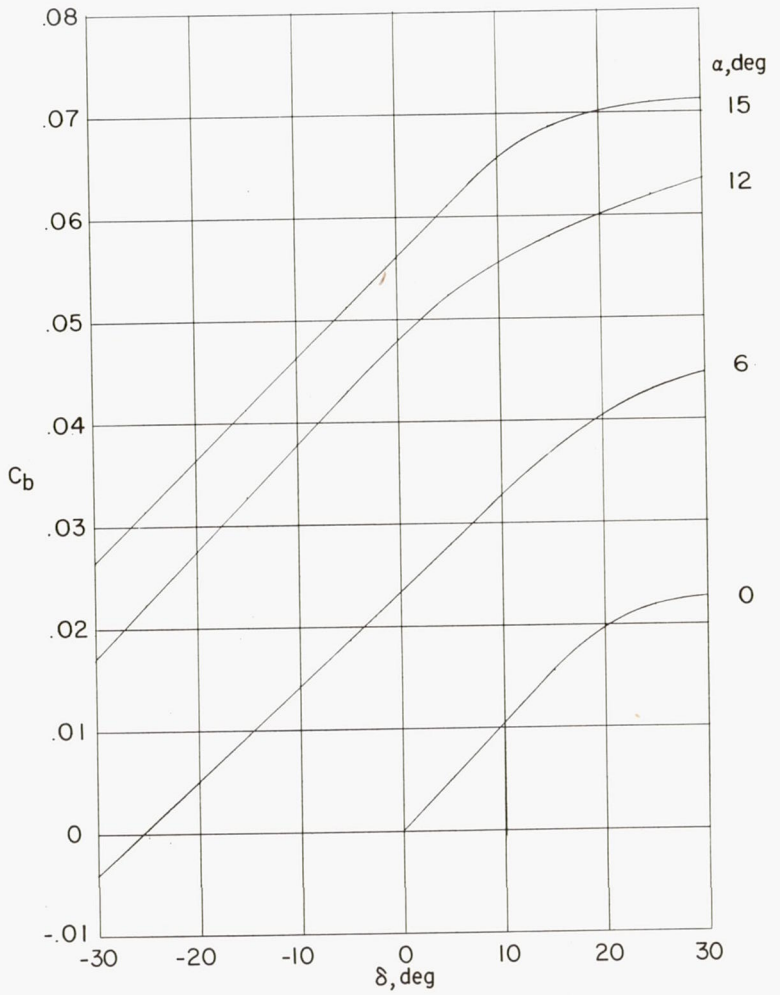

(b) C_b.

Figure 10.- Variation of basic coefficients with control deflection for configuration E.

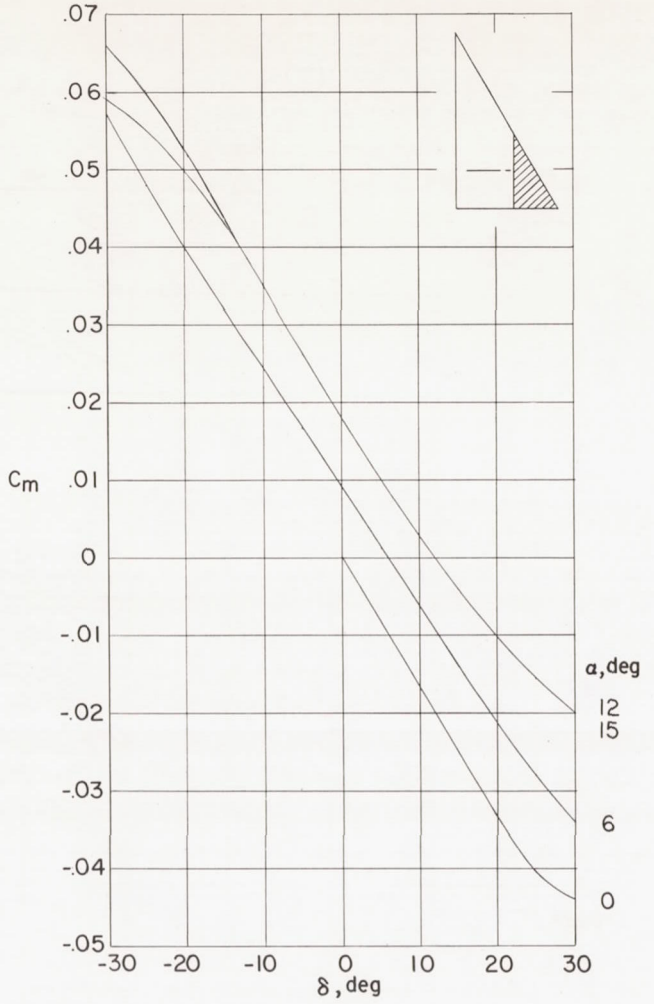

(c) C_m.

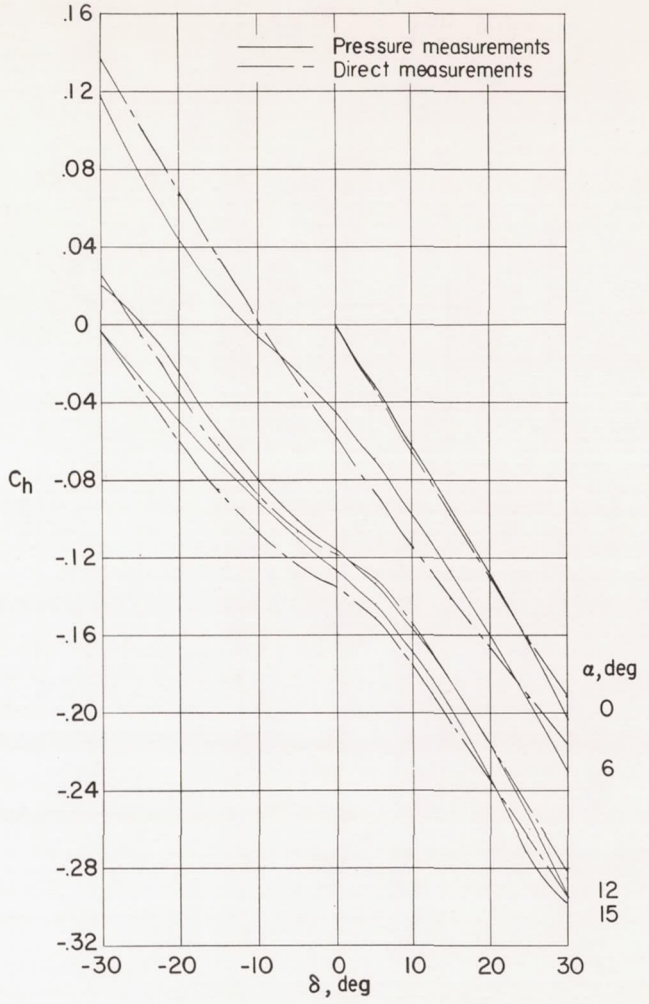

(d) C_h.

Figure 10.- Concluded.

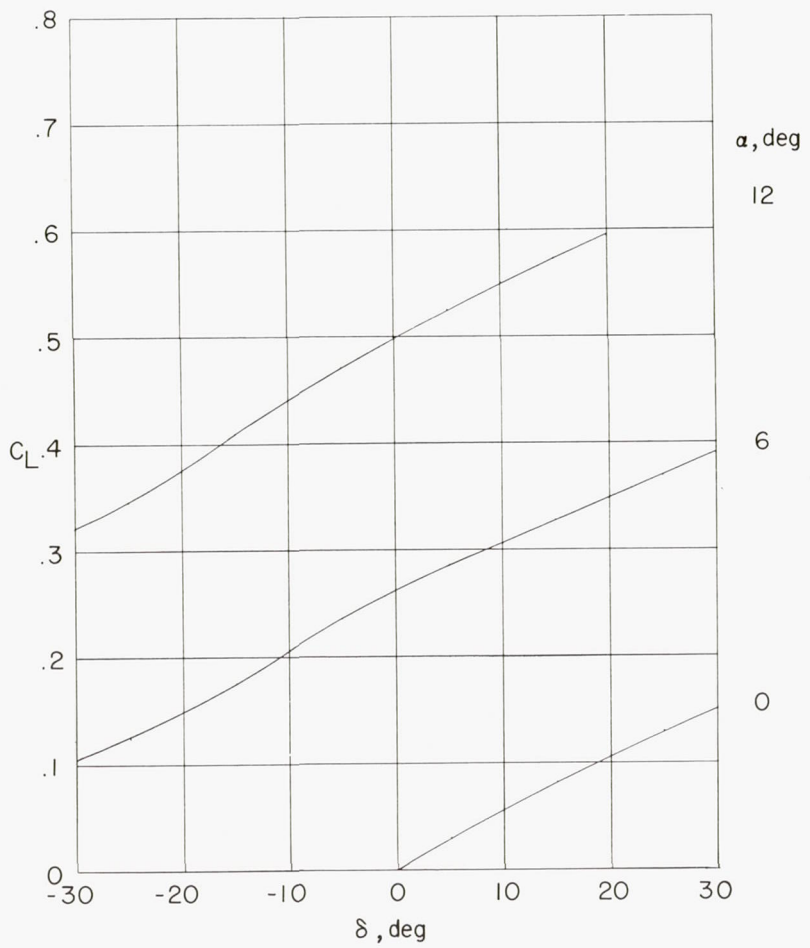

(a) C_L.

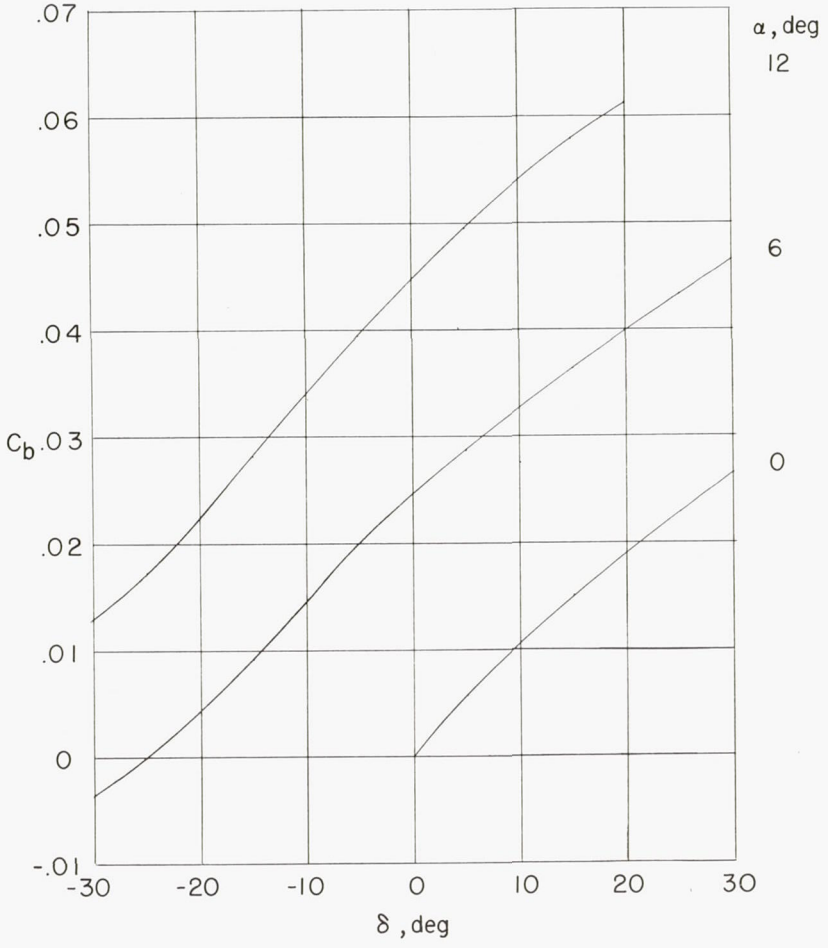

(b) C_b.

Figure 11.- Variation of basic coefficients with control deflection for configuration E with full-chord fence.

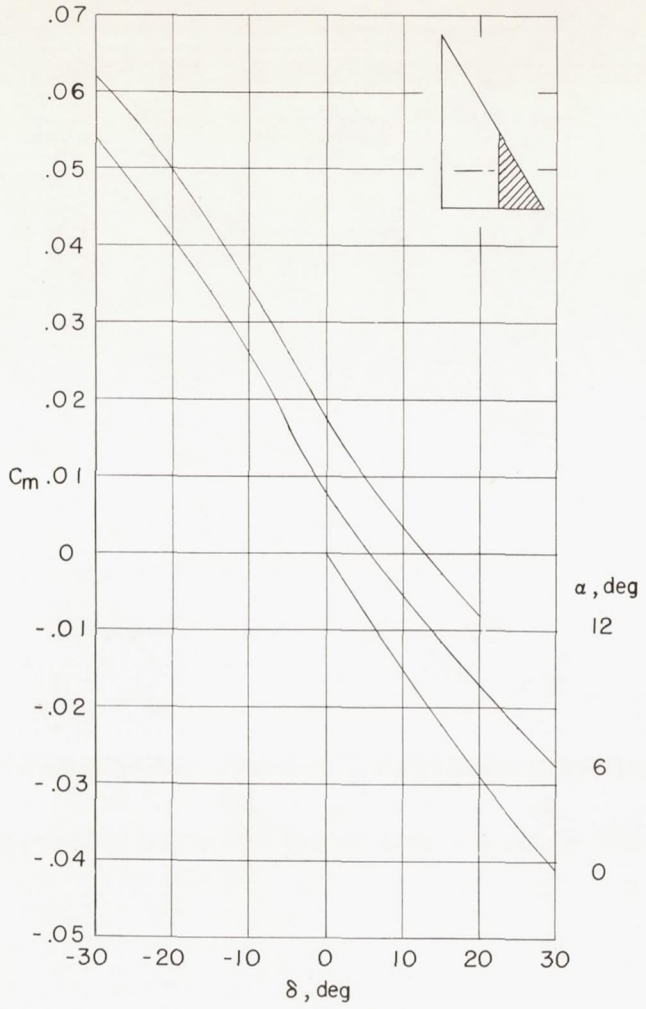

(c) C_m.

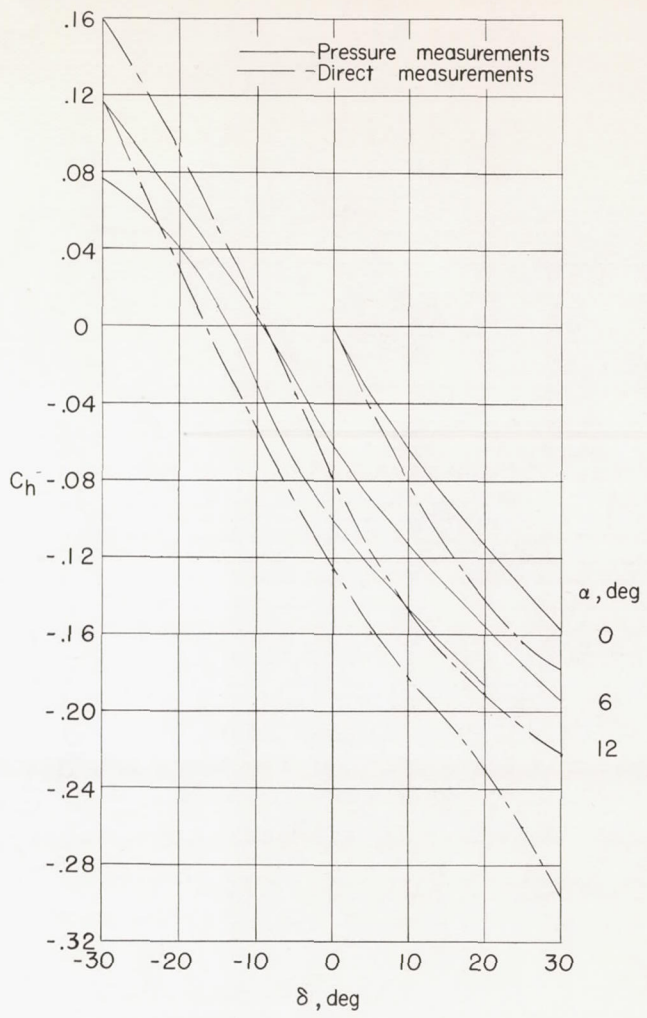

(d) C_h.

Figure 11.- Concluded.

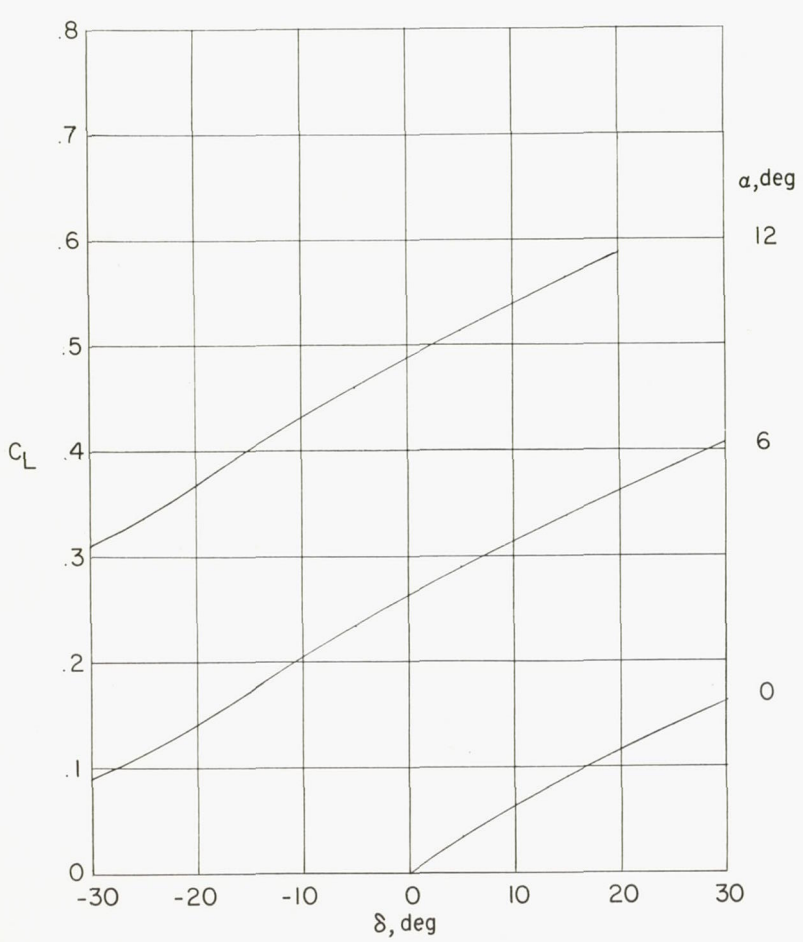

(a) C_L.

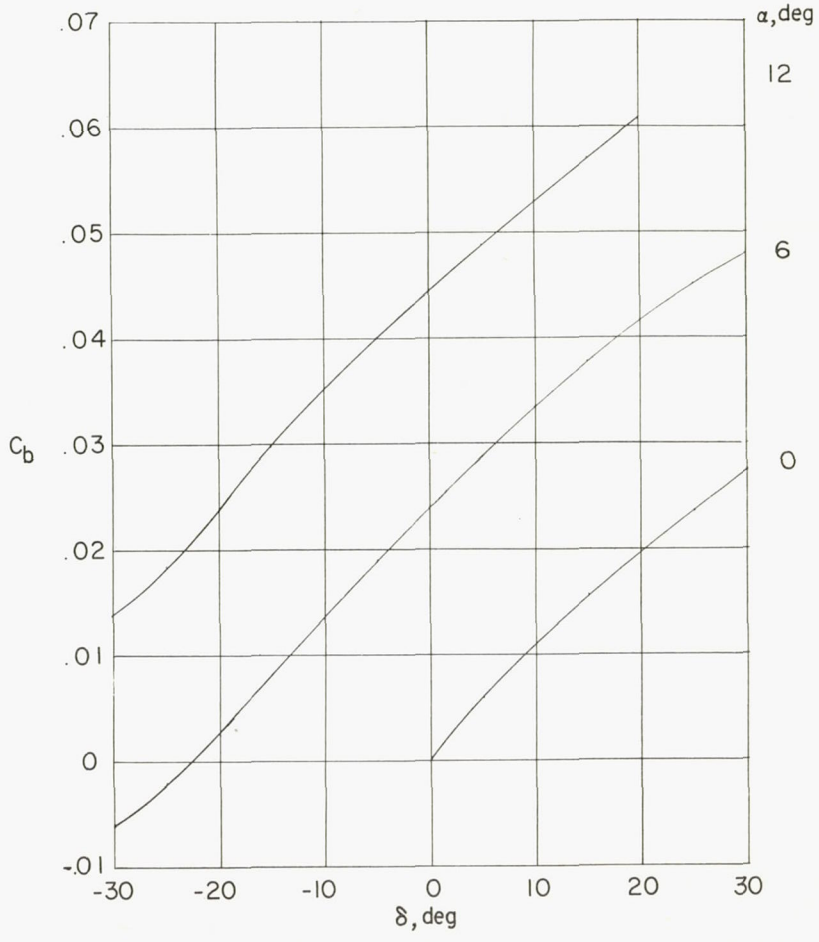

(b) C_b.

Figure 12.- Variation of basic coefficients with control deflection for configuration E with modified fence.

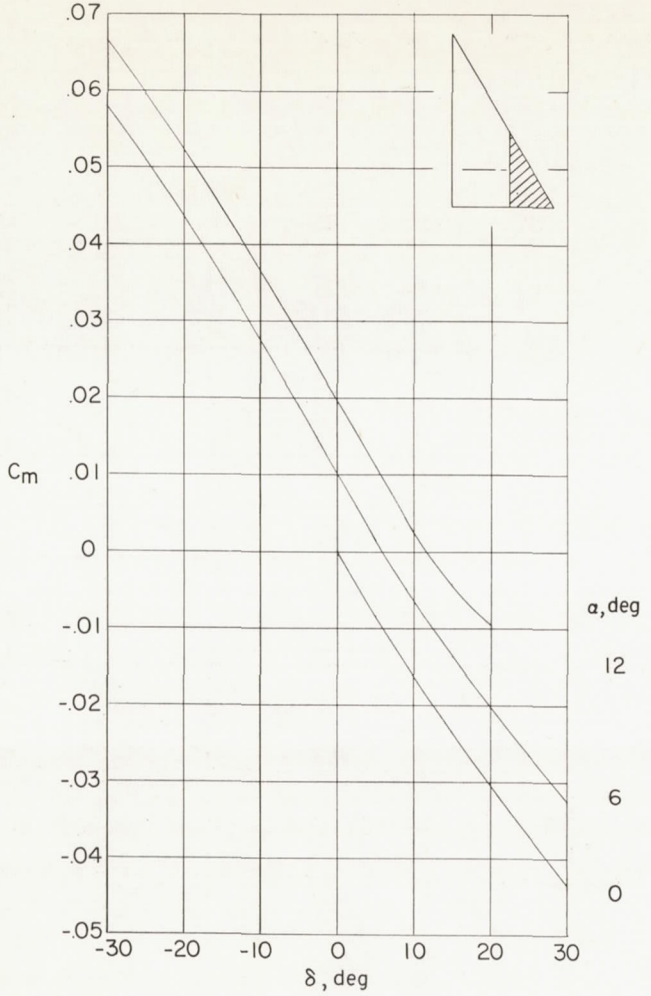

(c) C_m.

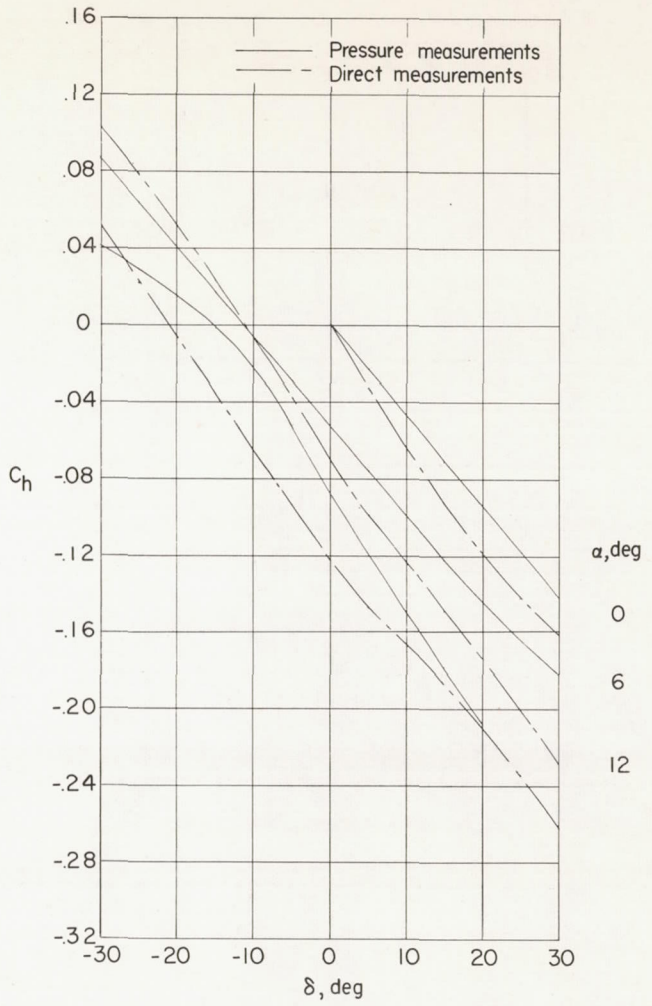

(d) C_h.

Figure 12.- Concluded.

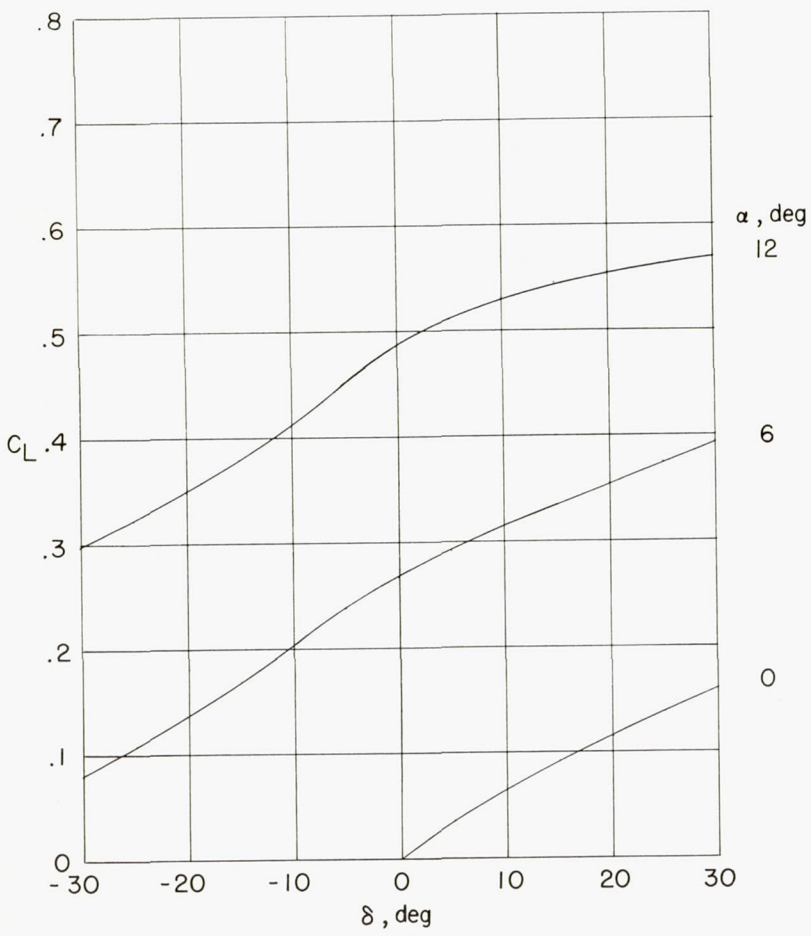

(a) C_L.

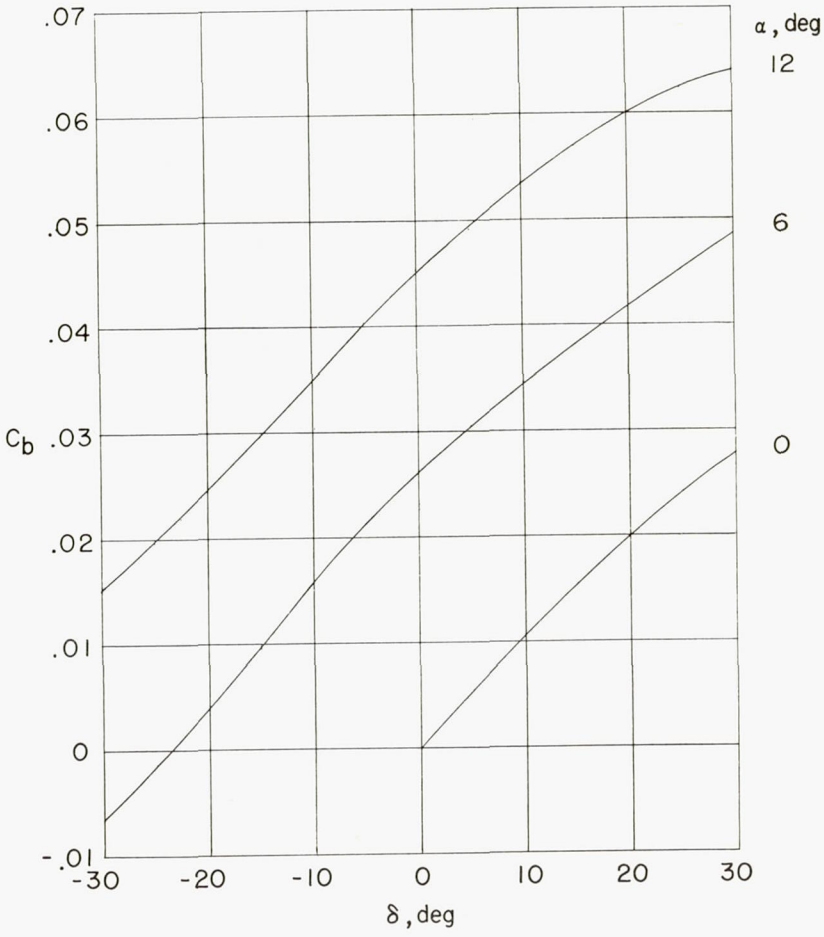

(b) C_b.

Figure 13.- Variation of basic coefficients with control deflection for configuration F.

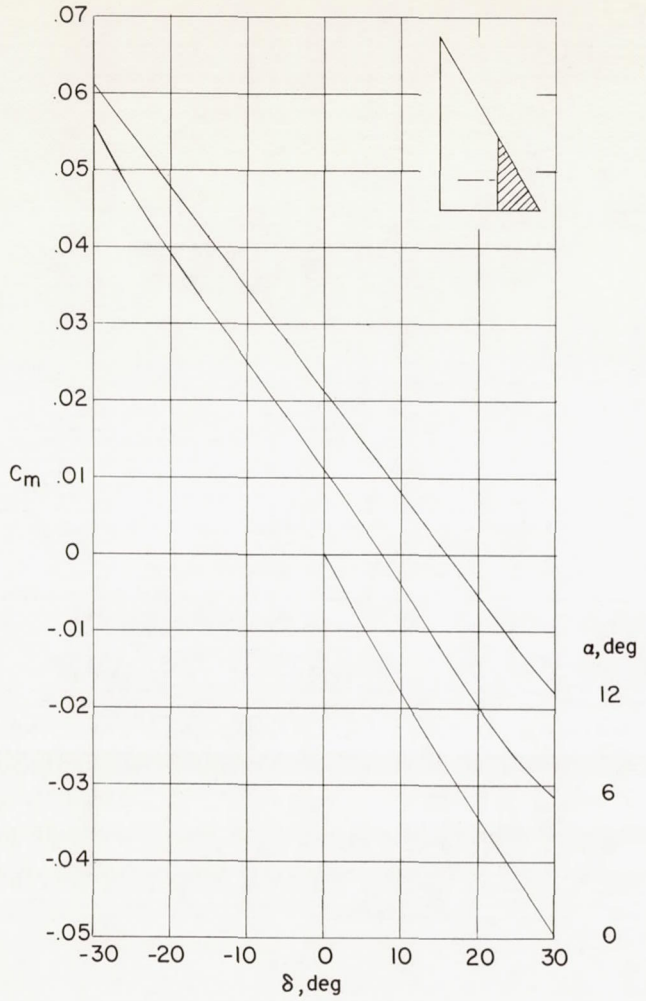

(c) C_m.

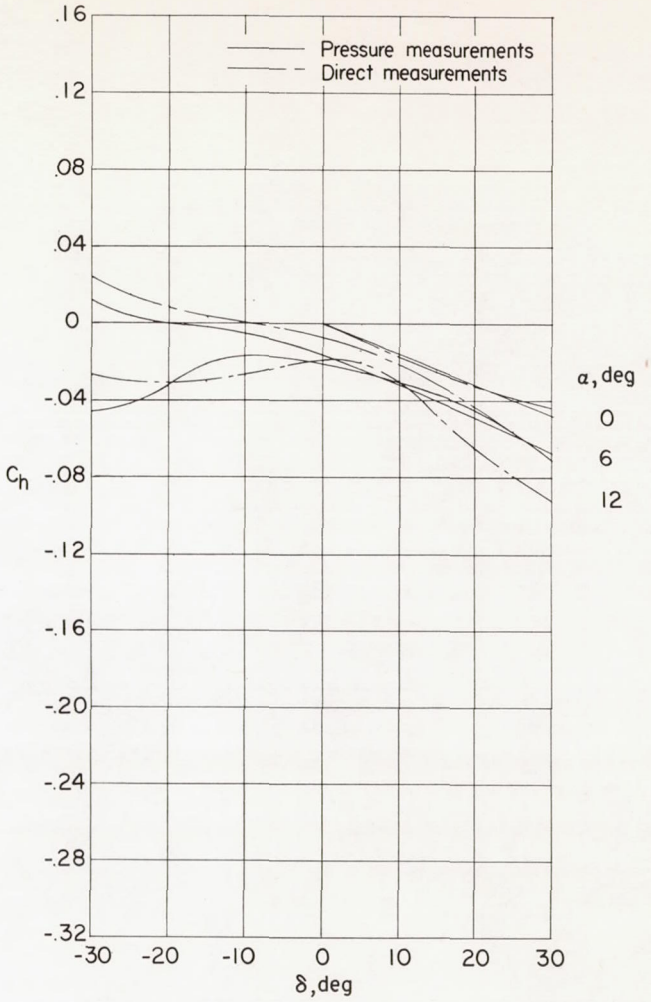

(d) C_h.

Figure 13.- Concluded.

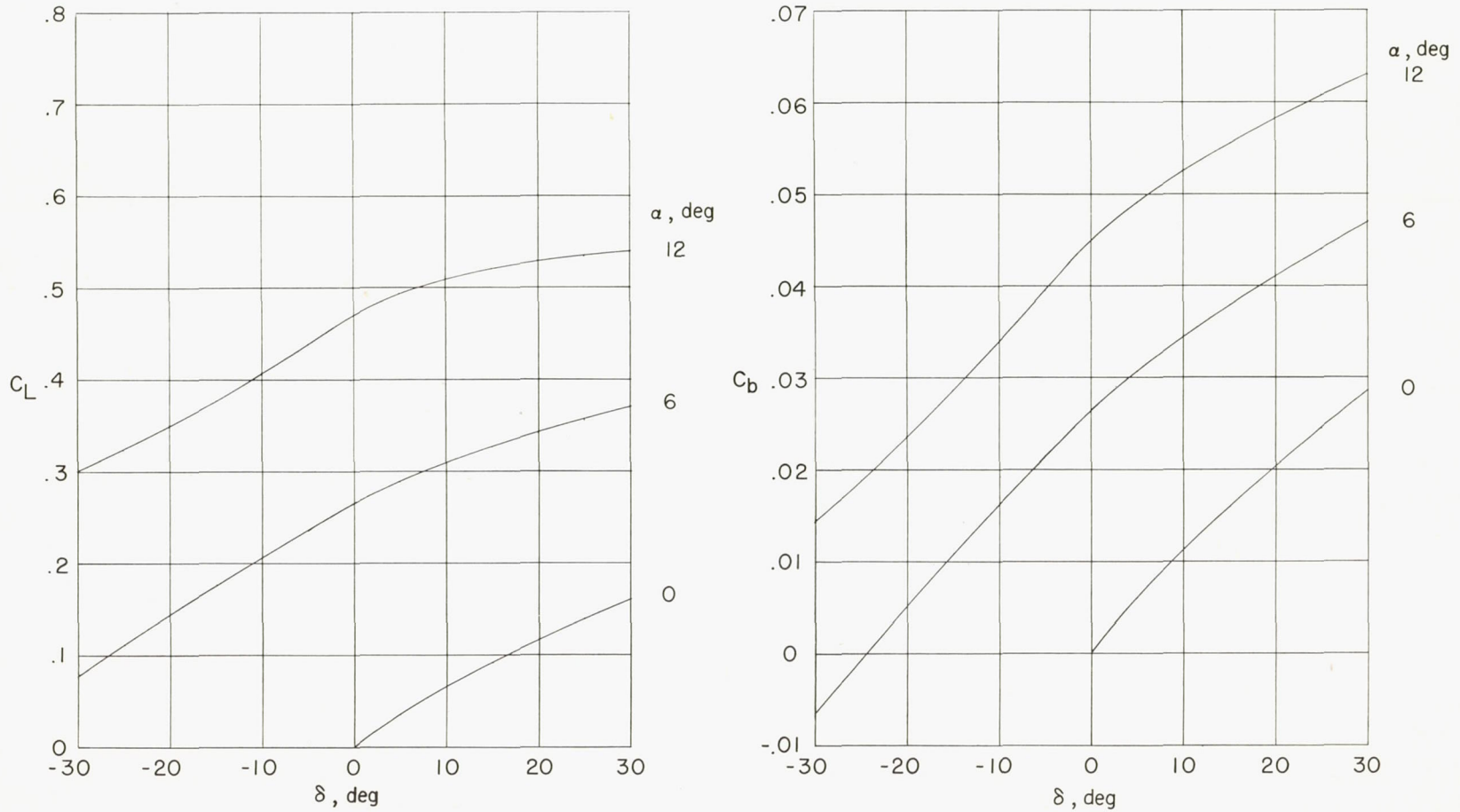

(a) C_L.

(b) C_b.

Figure 14.- Variation of basic coefficients with control deflection for configuration G.

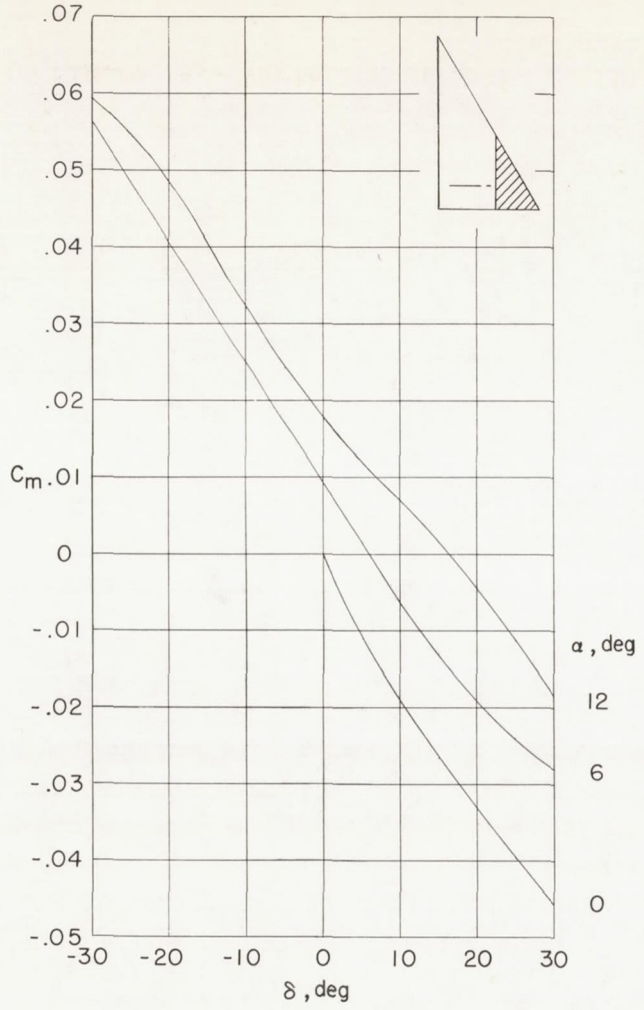

(c) C_m.

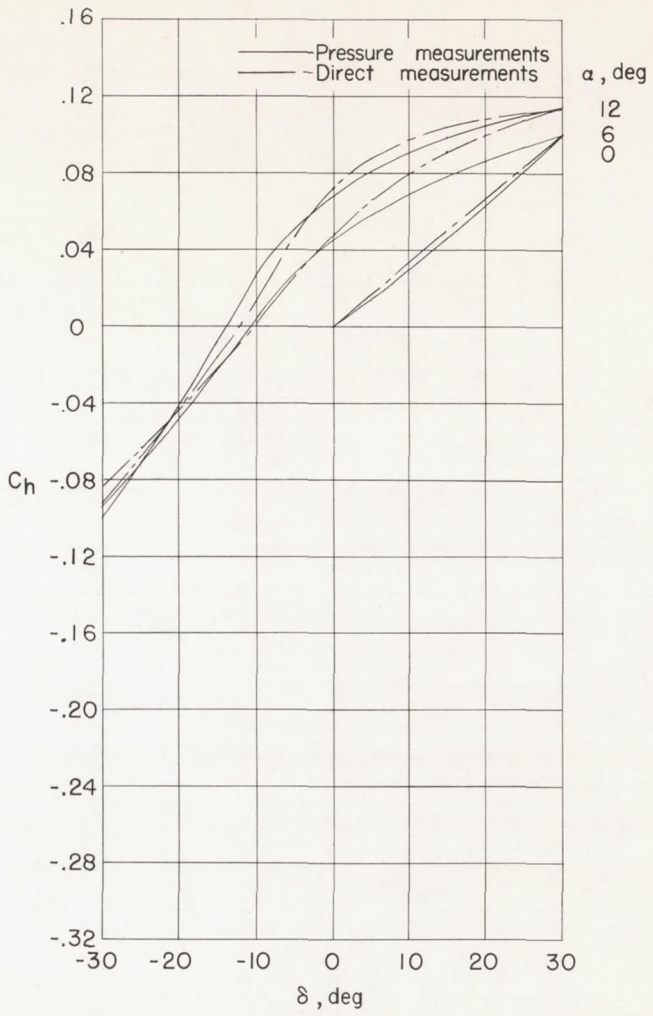

(d) C_h.

Figure 14.- Concluded.

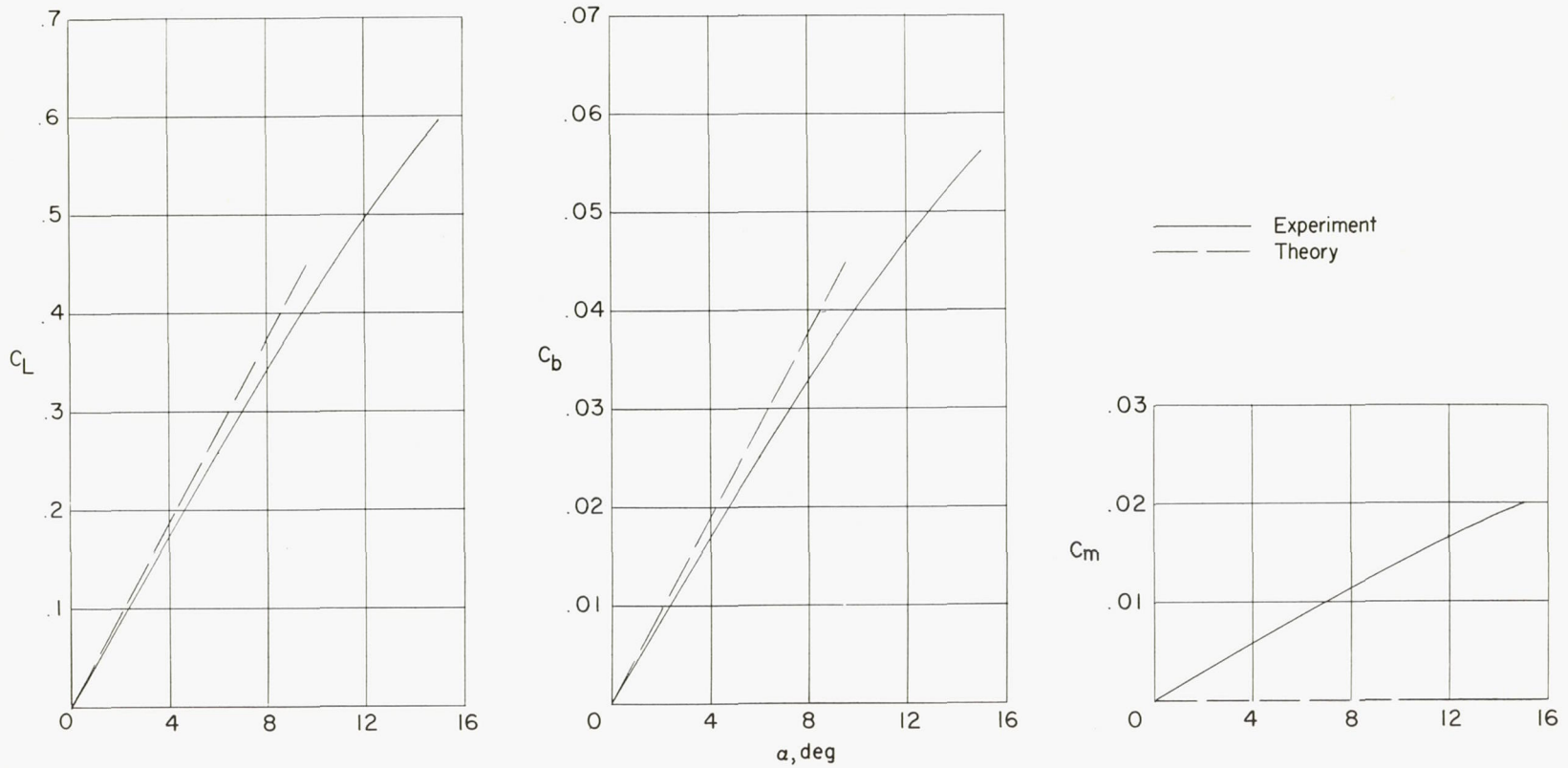

Figure 15.- Variations of wing lift, bending-moment, and pitching-moment coefficients with angle of attack. $\delta = 0^{\circ}$.

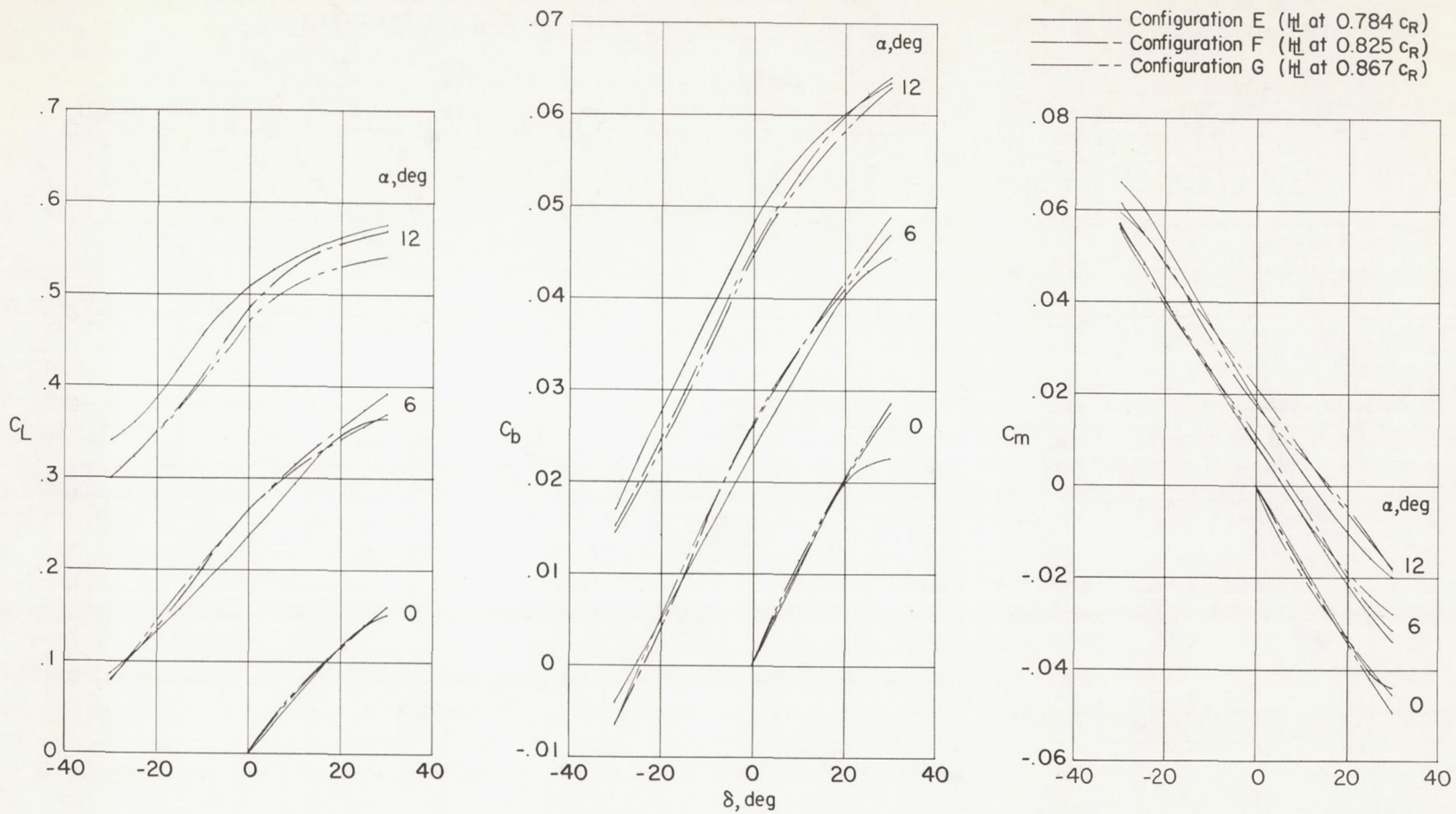

Figure 16.- Effect of moving the hinge line on the control effectiveness of the half-delta tip control.

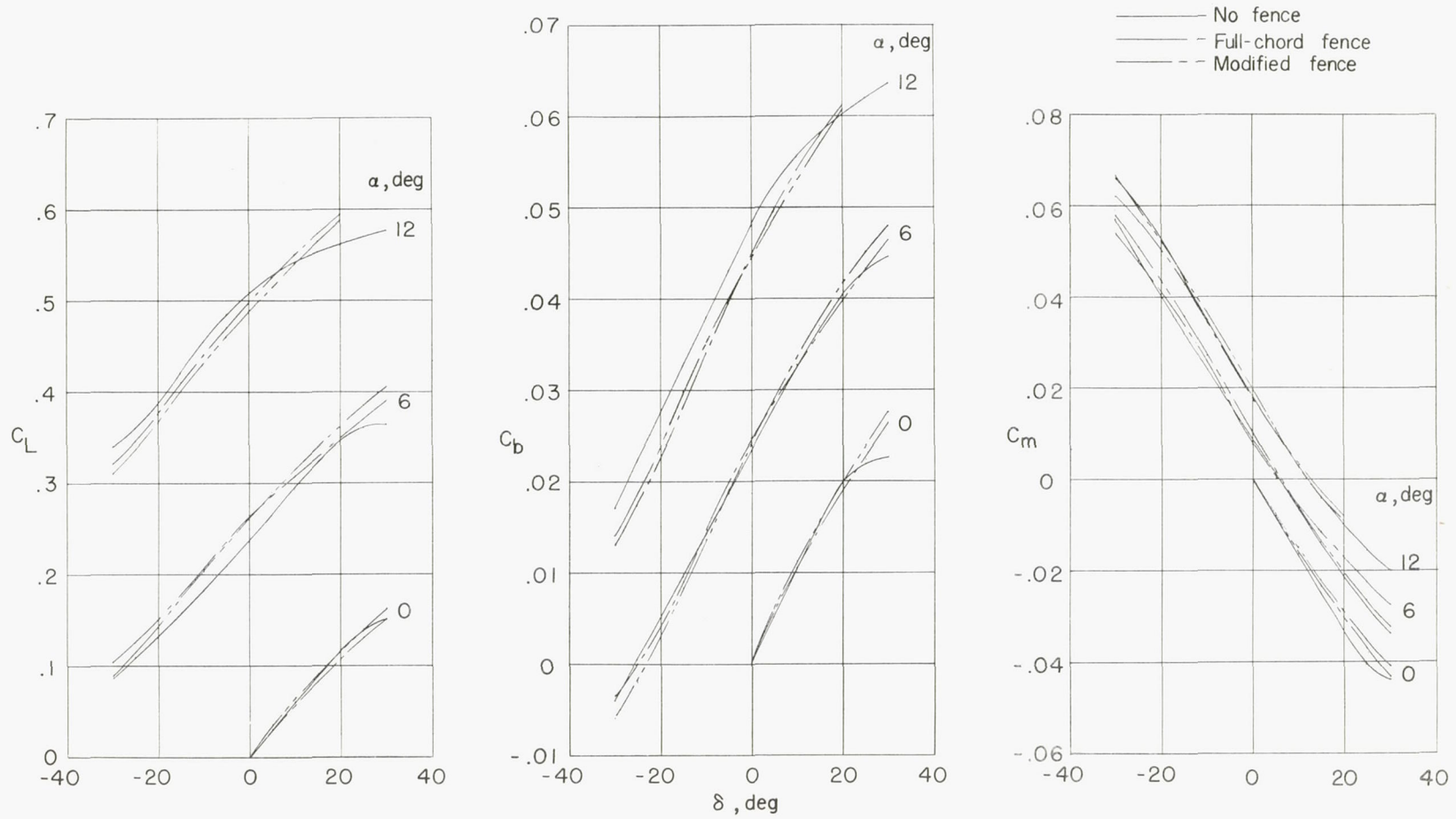

Figure 17.- Effect of the fences on the control effectiveness of configuration E.

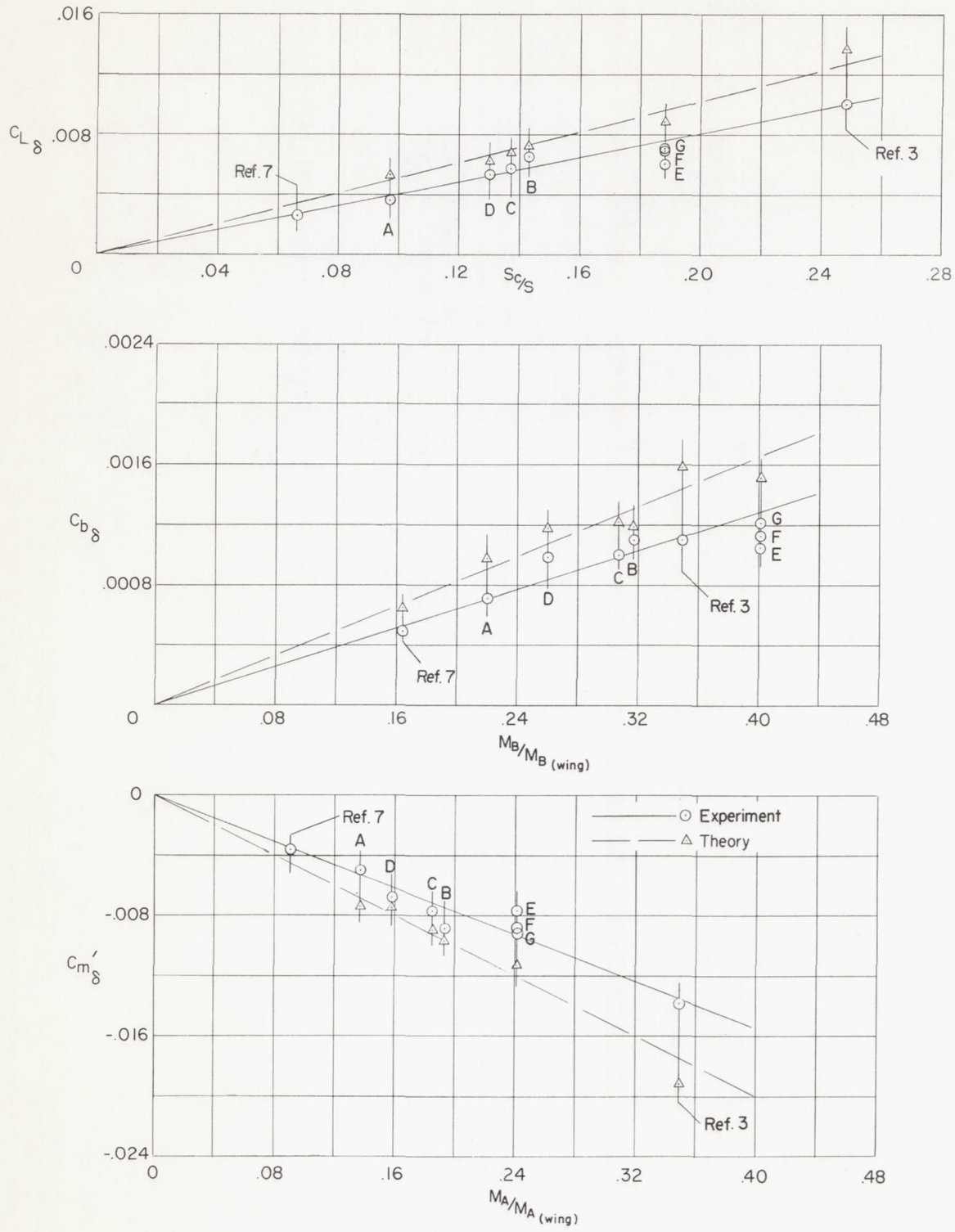

Figure 18.- Correlations of control effectiveness parameters with control areas and control-area moments.

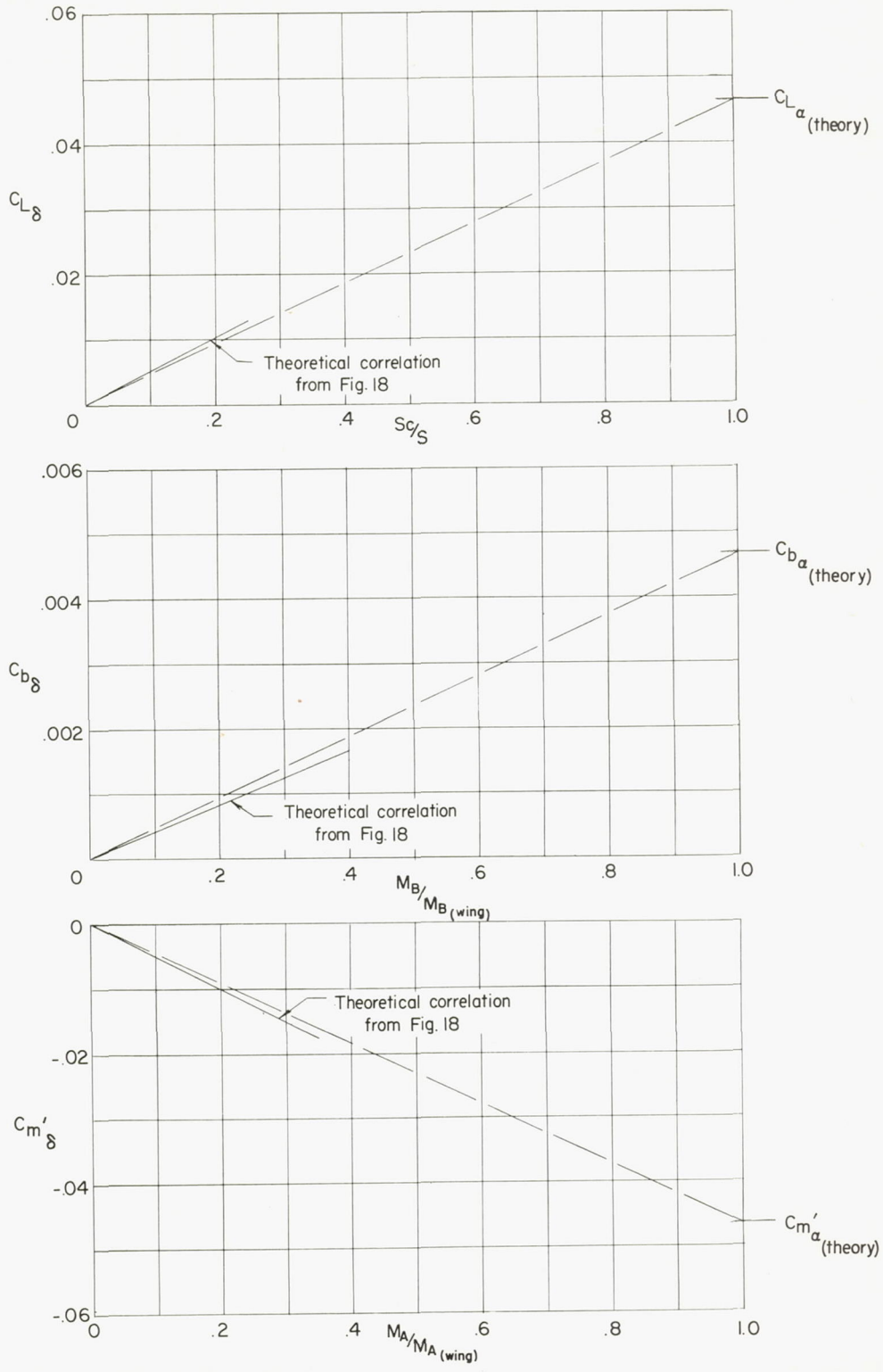

Figure 19.- Comparisons of theoretical control-effectiveness correlations with estimates determined from theoretical basic-wing characteristics.